Research Paper

GEOSPHERE

GEOSPHERE, v. 17

https://doi.org/10.1130/GES02346.1

11 figures; 1 table; 1 set of supplemental files

CORRESPONDENCE: tomas.capaldi@unlv.edu

CITATION: Capaldi, T.N., McKenzie, N.R., Horton, B.K., Mackaman-Lofland, C., Colleps, C.L., and Stockli, D.F., 2021, Detrital zircon record of Phanerozoic magmatism in the southern Central Andes: Geosphere, v. 17, https://doi.org/10.1130/GES02346.1.

Science Editor: Shanaka de Silva
Associate Editor: Christopher J. Spencer

Received 4 September 2020
Revision received 3 January 2021
Accepted 19 March 2021

Detrital zircon record of Phanerozoic magmatism in the southern Central Andes

T.N. Capaldi[1,*], N.R. McKenzie[2], B.K. Horton[1,3], C. Mackaman-Lofland[1], C.L. Colleps[2], and D.F. Stockli[1]

[1]Department of Geological Sciences, Jackson School of Geosciences, University of Texas at Austin, Austin, Texas 78712, USA
[2]Department of Earth Sciences, University of Hong Kong, Pokfulam Road, Hong Kong, China
[3]Institute for Geophysics, Jackson School of Geosciences, University of Texas at Austin, Austin, Texas 78712, USA

ABSTRACT

The spatial and temporal distribution of arc magmatism and associated isotopic variations provide insights into the Phanerozoic history of the western margin of South America during major shifts in Andean and pre-Andean plate interactions. We integrated detrital zircon U-Th-Pb and Hf isotopic results across continental magmatic arc systems of Chile and western Argentina (28°S–33°S) with igneous bedrock geochronologic and zircon Hf isotope results to define isotopic signatures linked to changes in continental margin processes. Key tectonic phases included: Paleozoic terrane accretion and Carboniferous subduction initiation during Gondwanide orogenesis, Permian–Triassic extensional collapse, Jurassic–Paleogene continental arc magmatism, and Neogene flat slab subduction during Andean shortening. The ~550 m.y. record of magmatic activity records spatial trends in magma composition associated with terrane boundaries. East of 69°W, radiogenic isotopic signatures indicate reworked continental lithosphere with enriched (evolved) εHf values and low (<0.65) zircon Th/U ratios during phases of early Paleozoic and Miocene shortening and lithospheric thickening. In contrast, the magmatic record west of 69°W displays depleted (juvenile) εHf values and high (>0.7) zircon Th/U values consistent with increased asthenospheric contributions during lithospheric thinning. Spatial constraints on Mesozoic to Cenozoic arc width provide a rough approximation of relative subduction angle, such that an increase in arc width reflects shallower slab dip. Comparisons among slab dip calculations with time-averaged εHf and Th/U zircon results exhibit a clear trend of decreasing (enriched) magma compositions with increasing arc width and decreasing slab dip. Collectively, these data sets demonstrate the influence of subduction angle on the position of upper-plate magmatism (including inboard arc advance and outboard arc retreat), changes in isotopic signatures, and overall composition of crustal and mantle material along the western edge of South America.

INTRODUCTION

Subduction zones are fundamental components of Earth systems that link lithospheric dynamics, mountain building, surface processes, magmatism, and climate–carbon cycles. Spatial, temporal, and compositional changes in continental arc magmatism in Cordilleran-type orogenic systems have been shown to be a function of variations in subduction dynamics and overriding plate processes (Dickinson, 1975; Haschke et al., 2002, 2006; Kay et al., 2005; Trumbull et al., 2006; Kirsch et al., 2016; Ancellin et al., 2017; de Silva and Kay, 2018; Chapman and Ducea, 2019). The southern Central Andes, spanning the modern retroarc region of central Argentina and forearc region of Chile (Fig. 1), represent one of the few places on Earth where a long-lived (>100 m.y.) convergent margin provides the magmatic record necessary to evaluate spatial-temporal relationships among geodynamic processes, upper-plate deformation, and subduction-related magmatism.

The South American plate at 28°S –33°S is composed of numerous north-south–trending terranes of variable composition that may have induced a spatial control on the geochemical signatures of subsequent Andean tectono-magmatic regimes (Chapman et al., 2017). A critical debate persists over the timing and geologic expression of subduction initiation along the South American margin after Paleozoic terrane accretion. Traditional models have attributed magmatic compositional changes to Triassic subduction shutoff during intraplate anorogenic and/or extensional conditions followed by Early Jurassic subduction initiation (Kay et al., 1989; Mpodozis and Kay, 1992; Llambías and Sato, 1995; Kleiman and Japas, 2009). Andean magmatic records that span from the Early Jurassic (ca. 200 Ma) to present provide a foundation for interpreting the history of Andean subduction and orogenesis (Haschke et al., 2002, 2006; Trumbull et al., 2006; Folguera and Ramos, 2011; Balgord, 2017; Faccenna et al., 2017; Schellart, 2017; Butler et al., 2019; Sundell et al., 2019; Spencer et al., 2019; Chen et al., 2019). Although best known for Cenozoic contractional orogenesis, the western margin of South America has experienced varied tectonic regimes throughout the Phanerozoic, potentially preserving an earlier phase of subduction-related magmatism that dates back to the Carboniferous (Alasino et al., 2012; Dahlquist et al., 2013; del Rey et al., 2016). For long-lived (>100 m.y.) Cordilleran orogenic systems, variations in the position of the magmatic arc have been variably linked to changes in the dip of the subducted slab, the rate of plate convergence, and/or magnitude of forearc

Tomas Capaldi https://orcid.org/0000-0003-4894-736X
*Now at Department of Geoscience, University of Nevada–Las Vegas, Las Vegas, Nevada 89154, USA.

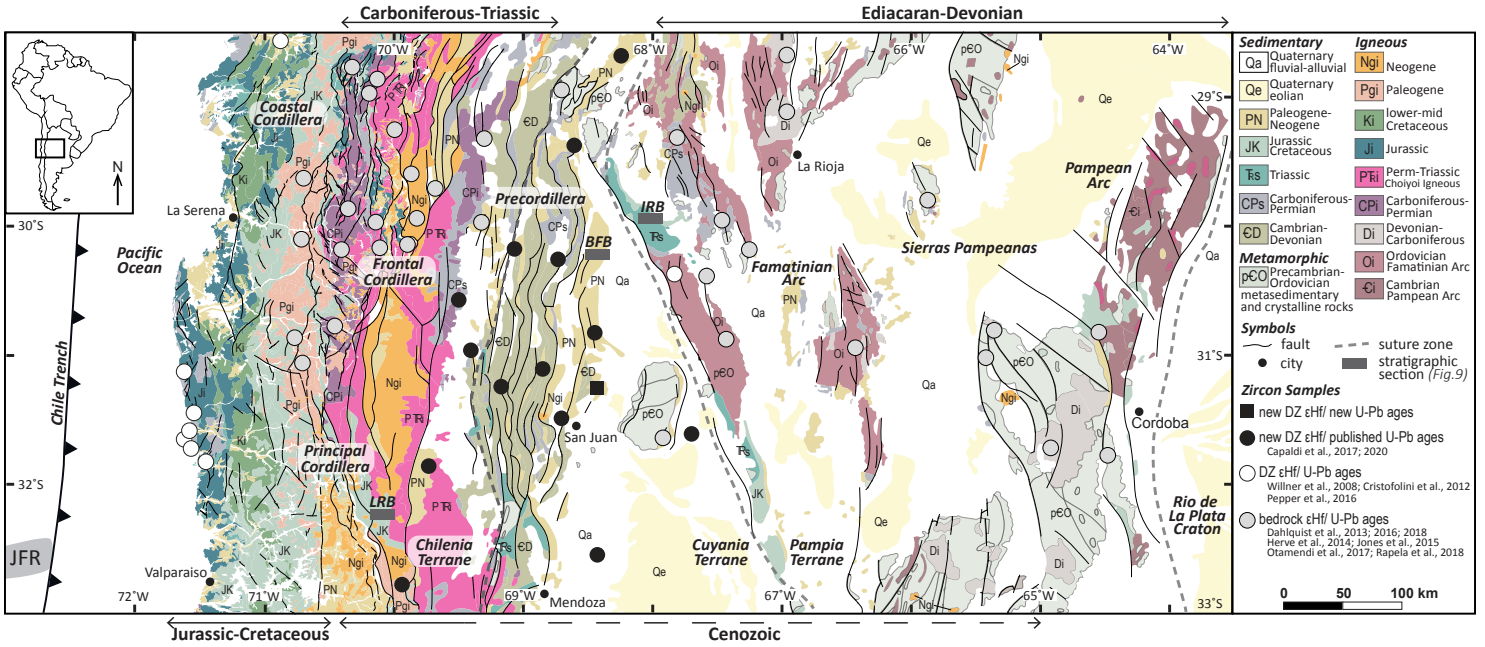

Figure 1. Geologic map of Argentina and Chile (28.5°S to 33°S) highlighting major Phanerozoic magmatic provinces, proposed terrane boundaries, and zircon sample locations. BFB—Bermejo foreland basin; IRB—Ischigualasto rift basin; LRB—La Ramada Basin; JFR—Juan Fernandez Ridge; DZ—detrital zircon (SEGEMAR, 1999, 2012; Sernageomin, 2003).

erosion (Ramos et al., 2002; Kay et al., 2005; Stern, 2011). Subduction angle has been interpreted to modulate mechanical coupling along subduction margins, control retroarc basin evolution, and drive phases of arc migration that are reflected in isotopic records (Ramos and Folguera, 2009; Horton, 2018a, 2018b; Chapman and Ducea, 2019). Evaluation of the operative spatial and temporal scales of trends in magmatic arc composition provides a means to assess proposals of high-flux events and magmatic lulls that may have generated cyclical or punctuated phases of arc magmatism (de Silva et al., 2015; Paterson and Ducea, 2015; Kirsch et al., 2016).

This study presents new detrital zircon U-Pb ages, U-Th ratios, and Lu-Hf isotopic data from modern river sands and sandstones throughout the retroarc region of central Argentina and forearc region of Chile (Fig. 1) to evaluate long-term (>100 m.y.), regional (>100 km scale) geologic patterns and changes in magmatic composition along the Andean margin. The detrital record provides valuable temporal controls on the evolution of upper-crustal composition (Condie et al., 2011; Cawood et al., 2012; Augustsson et al., 2016; Pepper et al., 2016; Balgord, 2017; Dhuime et al., 2017; McKenzie et al., 2018; Barber et al., 2019). Additionally, the spatial and temporal patterns in magmatism derived from compiled bedrock geochronological data sets provide constraints on magmatic arc width, from which we estimated average slab dip values for past subduction systems. Subduction angle can be calculated for a continental magmatic arc when the width of the arc and depth of melting are known (Fig. 2), assuming dehydration melting at a specific depth and vertical melt ascent (Keith, 1978, 1982; Peacock et al., 1994). To assess the relationships among arc width, subduction angle, and melting depth, we first characterized the modern geometry of the Nazca subduction zone, the spatial pattern of Andean arc magmatism, and the depth of melt generation. Integrated spatial, temporal, and compositional trends in magmatism enabled us to evaluate the spatial control on crustal geochemical signatures, timing of subduction initiation, and estimation of subduction angle variations along the transition between the central and southern Andes.

GEOLOGIC SETTING

Igneous and associated metamorphic rocks in Argentina and Chile (Fig. 1) can be divided into four distinct groups: (1) Ediacaran to Devonian basement rocks of the Sierras Pampeanas and eastern craton; (2) Carboniferous–Triassic rocks of the Frontal and Principal Cordilleras; (3) Jurassic–Paleogene rocks of the Coastal Cordillera; and (4) Cenozoic volcanic rocks that get younger eastward from the Principal Cordillera toward the Argentina foreland.

Latest Ediacaran to Devonian igneous and metamorphic belts are exposed across the Sierras Pampeanas. Key phases include the Pampean (555–515 Ma) and Famatinian (495–460 Ma) magmatic arcs, generated during east-dipping subduction (Ramos et al., 1986; Bahlburg et al., 2009). The Precambrian to Ordovician history included accretion of Laurentian terranes (including Cuyania) to the Gondwana margin, followed by the poorly constrained accretion of the Chilenia terrane (Ramos et al., 1984; Thomas et al., 2015; Rapela et al., 2016; Martin et al., 2019). Isolated granitic plutons of Devonian age across the Sierras Pampeanas region are interpreted to have been emplaced during extensional conditions (Dahlquist et al., 2013; Moreno et al., 2020).

Carboniferous–Triassic igneous complexes form much of the High Andes, with the Choiyoi igneous complex spanning the Principal Cordillera along the Chile-Argentina border and flanking regions to the west and east (Frontal Cordillera and parts of the Andean foreland). Batholith emplacement in the northern Frontal Cordillera involved many phases of Carboniferous to Triassic orogenic and postorogenic magmatism (Hervé et al., 2014; Sato et al., 2015). Late Carboniferous to early Permian magmatism was synchronous with growth of the NW-NNW–trending Gondwanide orogenic belt during east-dipping subduction (Giambiagi et al., 2014; Hervé et al., 2014). After the cessation of Gondwanide shortening and crustal thickening, the emplacement of calc-alkaline to alkaline bimodal intrusive suites and exceptionally thick (>5–10 km) ignimbrites of the Choiyoi Group (ca. 280–248 Ma) is consistent with crustal melting and possible postorogenic collapse prior to and during the earliest stages of Gondwana breakup (Mpodozis and Kay, 1992; Kleiman and Japas, 2009; Sato et al., 2015; Nelson and Cottle, 2019).

East-dipping subduction generated the Jurassic to Cenozoic Andean magmatic arc, which is defined by north-trending belts involving principally granite/granodiorite intrusions and andesite flows. These belts show a systematic eastward decrease in age, from Jurassic (200–165 Ma) and Cretaceous (130–90 Ma) rocks along the Chilean coast, to Paleocene–Eocene (67–38 Ma) and Eocene–Oligocene (27–18 Ma) units along the western flank of the Principal Cordillera, and finally Miocene (17–10 Ma) volcanic rocks in the eastern Principal Cordillera, Frontal Cordillera, and Argentine foreland (Parada et al., 1988, 1999; Kay et al., 1991; Haschke et al., 2006; Jones et al., 2016). Miocene magmatism was concurrent with significant (~150 km) retroarc crustal shortening largely focused in the Precordillera fold-and-thrust belt (Jordan et al., 1993; Allmendinger and Judge, 2014; Fosdick et al., 2015; Mosolf et al., 2019; Mackaman-Lofland et al., 2020). The modern Pampean segment of the Nazca–South American plate boundary is characterized by shallow subduction, an ~500-km-long gap in active volcanism, and foreland basement uplifts of the Sierras Pampeanas that persist >700 km toward the craton, potentially driven by subduction of the Juan Fernandez Ridge (Barazangi and Isacks, 1976; Jordan et al., 1983; Ramos et al., 2002; Ramos and Folguera, 2009; Alvarado et al., 2009).

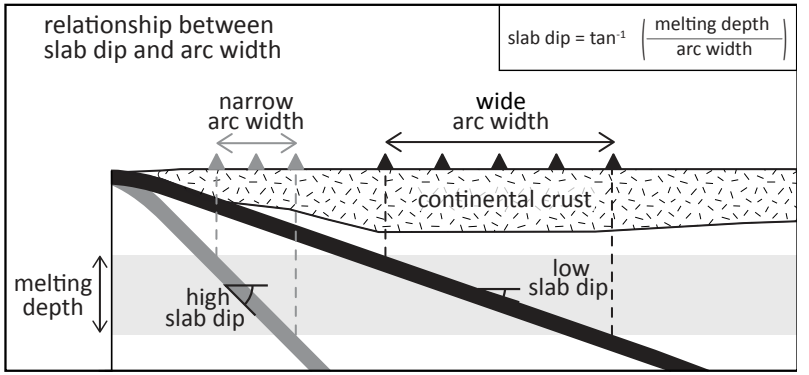

Figure 2. Schematic diagram illustrating relationships among continental arc width and dehydration melting in the asthenosphere as a function of subduction angle for narrow arcs (gray triangle) and wide arcs (black triangle).

METHODS AND RESULTS

Reconstructing Subduction Angle through Time

The angle of subduction influences the position of the magmatic arc, thermal structure of the mantle wedge, and stress conditions in the overriding plate. To constrain long-term variations in past subduction angle, we utilized the time-space distribution of arc magmatism following the simplified approach of Keith (1978, 1982) in which dehydration melting occurs at specific depths during vertical ascent of magma through the overriding plate (Fig. 2). Dehydration melting occurs in the upper mantle over a narrow range of depths defined as a melting window with finite upper and lower limits (Fig. 2). From this relationship, subduction angle can be calculated for a continental arc with a known arc width and melting depth. The arc width to slab dip relationship does not require estimates of the arc-trench gap (distance between the magmatic front and subduction trench-slope break), which is a function of both subduction duration and subduction angle (Dickinson, 1973; Coney and Reynolds, 1977; Jacob et al., 1977; Jarrard, 1986; Isacks, 1988).

Estimating Melting Depth for Modern Arc Volcanos

To identify the relationship of arc width to subduction angle, we first constrained the limits of the melting depth window beneath the modern Andean arc. Pleistocene to Holocene arc volcano locations were compared with the geometry of the subducted Nazca slab to extract values of arc width, slab dip, and slab depth directly below all

volcanic locations (Fig. 3). Volcano locations (n = 1344; see Table S2[1]) were derived from the Smithsonian Institution database (Global Volcanism Program, 2013) and a compilation of South American bedrock radiometric ages (Pilger, 2018). The geometry of the Nazca slab was constrained by geophysical data, which integrated active-source seismic data interpretations, receiver functions, local to regional seismicity catalogs, and seismic tomography models to characterize active global subduction zone geometries (Fig. 3; Slab2 model: Hayes et al., 2018). Comparisons between the position of Andean arc volcanic centers and Nazca slab depth provided the upper and lower limits on the depth of dehydration melting. From the compiled Andean arc segments, we derived a mean melting depth of 91–150 km (Fig. 3A; Table S3). This value is in agreement with the observed locations of modern dehydration melting and volcano locations above the expected slab depth determined from tomographic models of the subducting Nazca plate (Gilbert et al., 2006; Porter et al., 2012; Bianchi et al., 2013). Importantly, this data synthesis demonstrates a clear relationship for the modern magmatic arc in which progressively lower values of slab dips correlate with progressively greater width of the magmatic arc (Fig. 3B; Table S3).

Calculating Magmatic Arc Width

We utilized an extensive data set of igneous ages and locations between 28°S and 33°S and between 65°W and 72°W to reconstruct arc width through time. The spatial distribution of magmatism was constrained by an extensive compilation (n = 1409; Table S4) of Phanerozoic bedrock radiometric ages (Fig. 4A; Pilger, 2018). Using longitudinal variations in igneous age, the width of the magmatic arc can be estimated for Cenozoic and Mesozoic igneous activity, but Paleozoic reconstructions are hampered by limited constraints on Paleozoic deformation. The sample density allowed for Cenozoic–Mesozoic arc width to be calculated for 2 m.y. intervals, with the exception of the Early Jurassic (190–170 Ma) magmatic arc (Fig. 4B). These calculations included palinspastic restoration of Cenozoic Andean shortening, including ~100 km of shortening in the Precordillera fold-and-thrust belt, 10 km of shortening along the Frontal Cordillera, 15 km of shortening in the Principal Cordillera, and 10 km of shortening along the Coastal Cordillera (Cristallini and Ramos, 2000; Farías et al., 2008; Allmendinger and Judge, 2014). Restorations of shortening were integrated over the entire data set, assuming shortening occurred during the major phase of Andean shortening (since 20 Ma). From this relationship, subduction angle was calculated for the Mesozoic–Cenozoic Andean continental arc using the restored arc widths and melt depths of 91–150 km (Fig. 4C; Table S5).

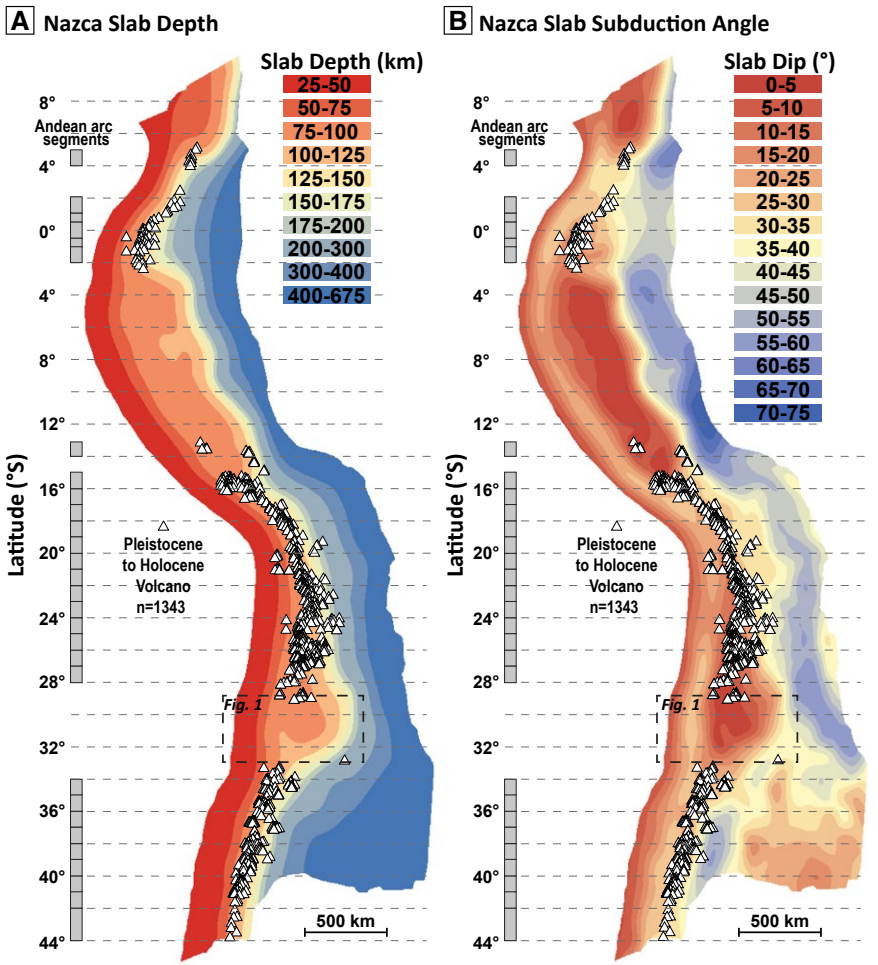

Figure 3. Map of Andean Pleistocene to Holocene volcanic centers compared to Nazca plate geometry (from Slab 2.0 models of Hayes et al., 2018). (A) Nazca plate depth from 25 to 675 km. (B) Nazca plate subduction angle between 0 and 75°.

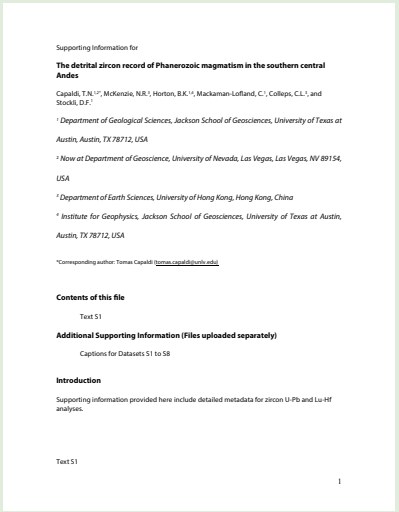

Supporting Information for

The detrital zircon record of Phanerozoic magmatism in the southern central Andes

Capaldi, T.N.[1,2*], McKenzie, N.R.[3], Horton, B.K.[1,4], Mackaman-Lofland, C.[1], Colleps, C.L.[1], and Stockli, D.F.[1]

[1] Department of Geological Sciences, Jackson School of Geosciences, University of Texas at Austin, Austin, TX 78712, USA

[2] Now at Department of Geoscience, University of Nevada, Las Vegas, Las Vegas, NV 89154, USA

[3] Department of Earth Sciences, University of Hong Kong, Hong Kong, China

[4] Institute for Geophysics, Jackson School of Geosciences, University of Texas at Austin, Austin, TX 78712, USA

*Corresponding author: Tomas Capaldi (tomas.capaldi@unlv.edu)

Contents of this file

Text S1

Additional Supporting Information (Files uploaded separately)

Captions for Datasets S1 to S8

Introduction

Supporting information provided here include detailed metadata for zircon U-Pb and Lu-Hf analyses.

Text S1

1

[1]Supplemental Material. Text S1: Analytical metadata. Table S2: Pleistocene–Holocene Andean volcanos and slab geometry. Table S3: Pleistocene–Holocene volcanic arc width and melt depth calculations. Table S4: Bedrock geochronology and location compilation. Table S5: Mesozoic–Cenozoic slab angle calculations. Table S6: Detrital zircon U-Th-Pb data. Table S7: Detrital zircon Hf data. Table S8: Detrital zircon U-Th-Pb data compilation. Table S9: Zircon Lu-Hf data compilation. Please visit https://doi.org/10.1130/GEOS.S.14251604 to access the supplemental material, and contact editing@geosociety.org with any questions. Readers can access new zircon Lu-Hf and U-Pb data by name, sample location, and analyses type at geochron.org (https://www.geochron.org/results.php?pkey=29370) and in the supporting information (Tables S2–S9). Site licensed under Creative Commons Attribution Noncommercial-Share Alike 3.0 and part of the IEDA Data Facility.

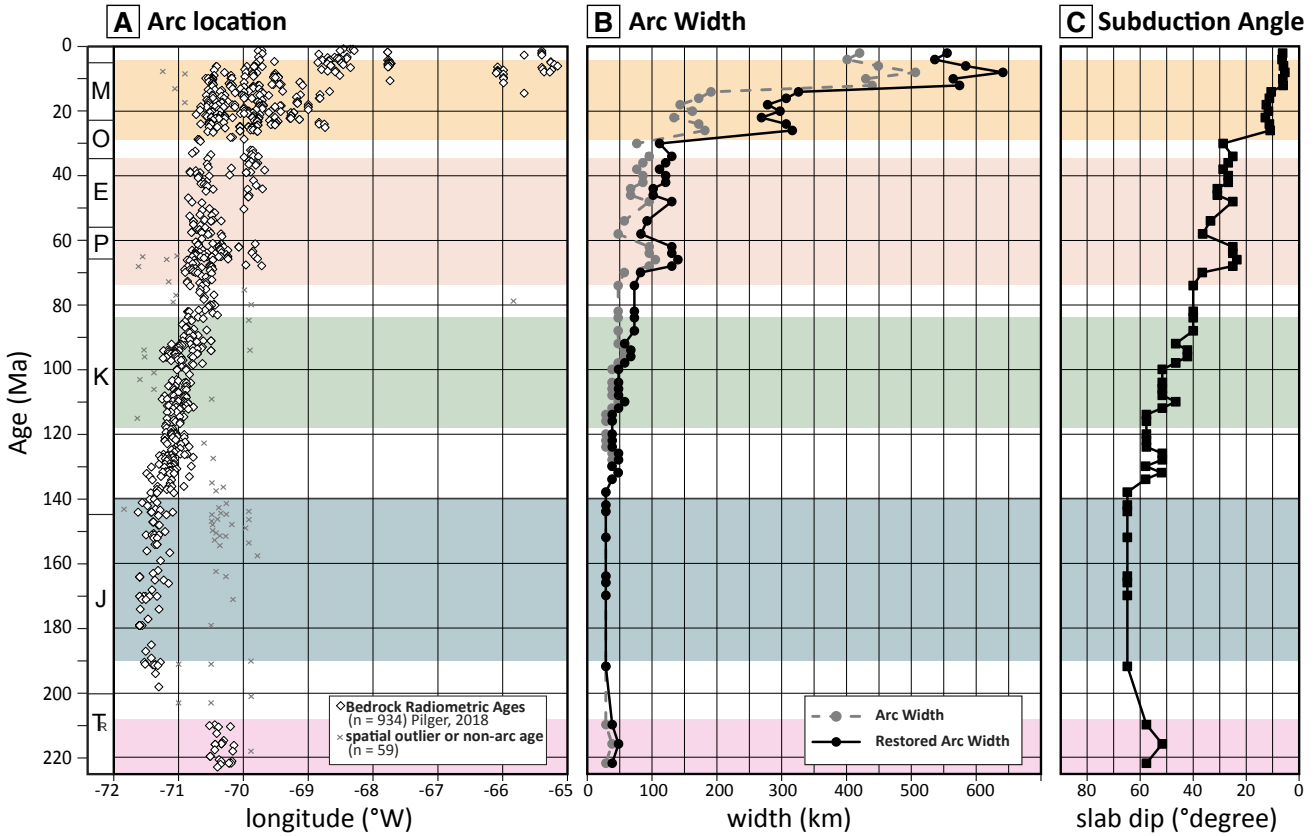

Figure 4. Comparisons among Mesozoic–Cenozoic Andean arc location, arc width, and subduction angle along Argentina and Chile (28.5°S to 33°S). (A) Bedrock radiometric ages (white diamonds) showing the time-space variations by sample longitude (°W) location (Pilger, 2018), and spatial outliers and nonarc ages (gray x symbols). (B) Arc width calculations for 2 m.y. intervals (gray dashed line) and palinspastic restoration of Cenozoic Andean shortening (black line). (C) Subduction angle calculations from corrected arc width estimates. T_R—Triassic; J—Jurassic; K—Cretaceous; P—Paleocene; E—Eocene; O—Oligocene; M—Miocene.

Results: Arc Width and Subduction Angle Trends

The long-term relationship between reconstructed Mesozoic to Cenozoic subduction angle and magmatic arc width shows the following trends: narrow (<50 km) arc widths associated with >50° subduction angles; moderate (50–150 km) arc widths associated with 20°–50° subduction angles; and wide (>300 km) arcs associated with <20° subduction angles (Figs. 4B and 4C). A clear temporal decrease in slab dip is apparent from the calculations (Fig. 4C). Triassic to Jurassic slab dips were the highest (50°–70°), followed by decreasing Cretaceous to early Cenozoic values (from 60° to 25°), and thereafter low Oligocene–Miocene values (from 15° to 10°) decreasing to 5° by Miocene–Pliocene time (Fig. 4C), in agreement with estimates for the modern Pampean flat slab geometry (Fig. 3B).

Caveats in Calculating Subduction Angle

Although the width of a magmatic arc strongly correlates with subduction angle, our simple reconstruction involves several caveats. (1) The calculations assumed subvertical ascent of fluids and magmas from the zone of melting, which may be oversimplified for shorter time frames (Schurr et al., 2003; Trumbull et al., 2006). (2) Andean arc migration has been associated with extensive (35–85 km)

forearc erosion and removal of trench-proximal (mostly Mesozoic) materials (Rutland, 1971; Coira et al., 1982; Kay et al., 2005; Stern, 2011), potentially resulting in an underrepresentation of true arc width for Mesozoic time steps. This approach does not explicitly account for episodes of forearc erosion, which would affect the position of the arc, but not the width. However, we note that any episode of forearc erosion that was accompanied by a shallowing in the dip of the subducted slab would be registered as an increase in arc width, per the relationship in Figure 4. (3) Older igneous materials may be covered or overprinted by younger volcanic events, limiting the extent of older outcrops and associated ages, which may limit arc width estimates for older time steps. (4) Major phases of intraplate Mesozoic volcanism occurred coeval with continental arc activity and were excluded from the calculations because their genesis far inboard from the subduction boundary was not related to slab dehydration melting (Fig. 4A). We used geochemical evidence (Rossel et al., 2013) and the spatial distribution to remove Jurassic (175–140 Ma) backarc magmatism from the arc width reconstruction. (5) Present-day flat slabs are principally characterized by the cessation of arc magmatism, such that our modern comparison between subduction angle and arc width lacks constraints for flat slab (<10° dip) segments. These caveats suggest that our calculations provide minimum values for arc width, which would generate modestly higher values of past subduction angle.

Detrital Zircon Geochronology and Geochemistry

U-Th-Pb Geochronology

Zircon is a highly refractory accessory mineral that most commonly forms in intermediate to felsic igneous assemblages and high-grade metamorphic rocks and incorporates relatively high concentrations of U and Hf (typically hundreds of parts per million) with very low amounts of common Pb (Gehrels, 2014; Schoene, 2014). Zircon Th/U ratios increase with decreasing SiO_2 content, such that zircons from granitic rocks have distinctly lower ratios (0.55–0.80) than zircons from gabbroic rocks (0.8–1.2; Kirkland et al., 2015; Yakymchuk et al., 2018). Zircon Th/U values can also serve as proxies for tectonic regime. Extensional phases have been associated with zircons with wide a range of Th/U values, including significant populations of elevated Th/U zircon (>1.0) produced by hotter magmas (700 to >1000 °C) with increased fractionation from more primitive mafic melts (Kirkland et al., 2015; McKay et al., 2018). In contrast, low Th/U values (<0.5) with limited geochemical variability correspond to phases of contractional orogenesis (Kemp et al., 2009; Rubatto, 2017; McKay et al., 2018).

Zircon U-Th-Pb analyses were conducted on Miocene sandstone samples from the Andean foreland. They record erosion from an extensive drainage area that includes Cenozoic volcanic rocks, Carboniferous–Triassic igneous rocks, and Paleozoic sedimentary rocks (Figs. 5A and 5B; Capaldi et al., 2020). Mineral separation included crushing, grinding, and water table, heavy-liquid density, and magnetic susceptibility separations. Nonmagnetic heavy mineral separates were poured onto double-sided tape on 2.5-cm-diameter epoxy resin mounts, and then zircon grains were chosen randomly for analysis by laser ablation–inductively coupled plasma–mass spectrometry (LA-ICP-MS) to determine Th/U isotopic ratios and obtain zircon U-Pb ages. Sample mounts were loaded into a large-volume Helex sample cell and ablated using a PhotonMachine Analyte G.2 excimer laser for analysis with a single-collector, magnetic sector Element2 ICP-MS at the University of Texas at Austin UTChron laboratory (Horton et al., 2015; Odlum et al., 2019). Corrections for depth-dependent, elemental and isotopic fractionation were performed using zircon standard GJ1 (600.4 ± 0.1 Ma; Jackson et al., 2004), yielding a concordia U-Pb age of 600.46 ± 0.7 Ma (mean square of weighted deviates [MSWD] = 0.52; $n = 67$). Secondary standards were analyzed periodically to verify the accuracy of the analyses; these included the Plesovice zircon (PL-1; 337.2 ± 0.4 Ma; Sláma et al., 2008), yielding a concordia U-Pb age of 339.3 ± 3.6 Ma (MSWD = 5.5; $n = 9$), and Pak-1 (43.03 Ma; in-house standard), yielding a concordia U-Pb age of 41.7 ± 0.5 Ma (MSWD = 2.8; $n = 8$). Zircon U-Pb ages and 2σ errors are reported as $^{206}Pb/^{238}U$ ages and $^{206}Pb/^{238}U$ versus $^{207}Pb/^{235}U$ discordance for analyses with less than 10% $^{206}Pb/^{238}U$ uncertainties, less than 20% discordance, and less than 5% reverse discordance (Table S6).

Lu-Hf Geochemistry

Zircon Hf isotopic compositions are sensitive to source rock type and crystallization environment, and they have been used to reconstruct the geochemical evolution of continental crust (Belousova et al., 2002, 2010; Kemp et al., 2006). Zircon Hf isotopic data are reported in epsilon units (ε) and presented in Hf evolution diagrams as εHf values representing the isotopic composition at the time of crystallization U-Pb age in reference to chondritic uniform reservoir (CHUR; Bouvier et al., 2008) and depleted mantle (DM; Vervoort and Blichert-Toft, 1999). Positive εHf values reflect juvenile crustal material originating from melts of depleted mantle origin, while negative εHf values are indicative of enriched melts derived from older recycled crustal material (Hildreth and Moorbath, 1988; Belousova et al., 2002; Hawkesworth and Kemp, 2006; Kemp et al., 2009). Studies of convergent margins have argued that a relative increase in zircon εHf is indicative of an extensional system characterized by outboard arc retreat during slab rollback and associated crustal thinning (Kemp et al., 2009; Spencer et al., 2019).

To characterize the isotopic composition of Phanerozoic magmatism, Hf geochemical analyses were conducted on detrital zircon grains with new and previously reported U-Pb age constraints (Figs. 5C; Tables S3 and S4; Levina et al., 2014; Capaldi et al., 2017, 2020). Numerous zircon grains were selected from each major U-Pb age component and then subjected to isotopic analysis by multicollector (MC) LA-ICP-MS at the University of Hong Kong. Zircon Lu-Hf-Yb isotopes were measured on a Nu Plasma high-resolution (HR) MC-ICP-MS coupled with a 193 nm excimer laser-ablation system (RESOlution M-50) by placing a 55-µm-diameter spot over the original U-Pb ablation pit following methods outlined in previous studies (Xia et al., 2011), and using zircon standards GJ1 (Elhlou et al., 2006) and 91500 (Wu et al., 2006; Table S7). Zircon standard 91500 yielded an average $^{176}Hf/^{177}Hf$ value of 0.282307 ± 0.00007

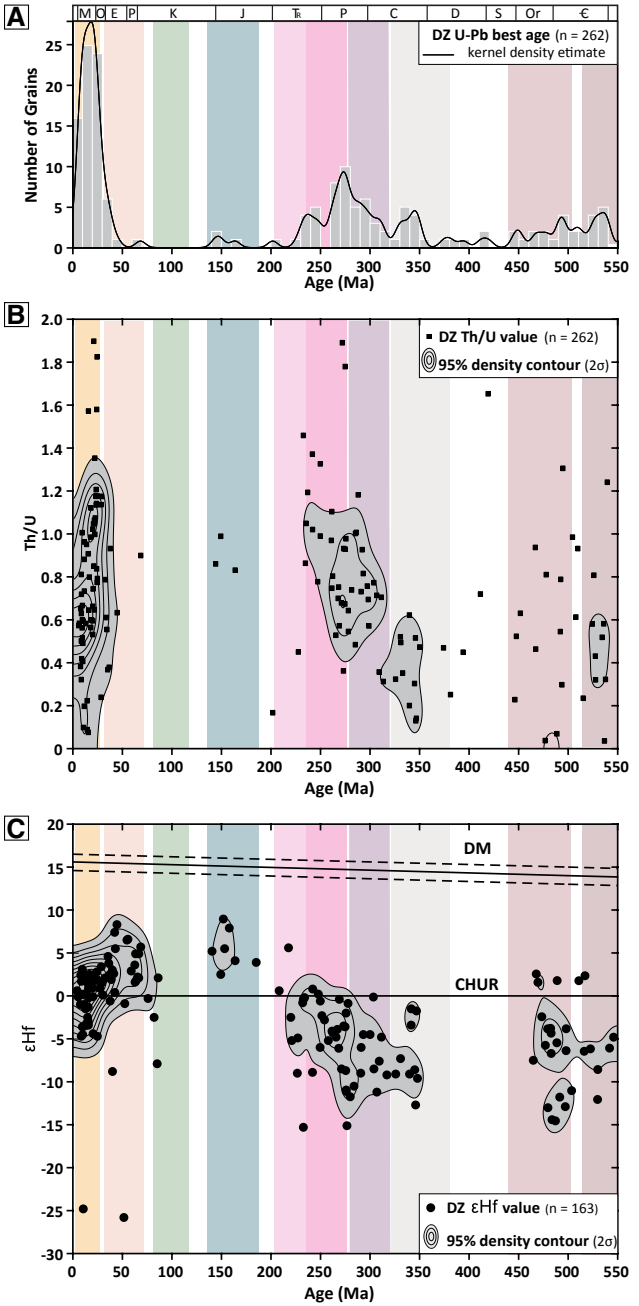

Figure 5. Detrital zircon (DZ) radiogenic isotopic data from Argentina. (A) Detrital zircon U-Pb age distributions from Argentina retroarc samples. (B) Two-dimensional (2-D) view of combined U-Pb age–Th/U results plotted as bivariate kernel density estimates for zircons (10 m.y. and 0.1 Th/U unit set kernel bandwidths). (C) Two-dimensional (2-D) view of combined U-Pb age–εHf results plotted as bivariate kernel density estimates for zircons younger than 550 Ma (10 m.y. and 2ε unit set kernel bandwidths) from Argentina retroarc. DM—depleted mantle; CHUR—chondritic uniform reservoir. Intensity contour plot represents 95% of the maximum intensity. Date were plotted using IsoplotR software (Vermeesch, 2018) and Hafnium Plotter software (Sundell et al., 2019). Є—Cambrian; Or—Ordovician; S—Silurian; D—Devonian; C—Carboniferous; P—Permian; T_R—Triassic; J—Jurassic; K—Cretaceous; P—Paleocene; E—Eocene; O—Oligocene; M—Miocene.

(MSWD = 0.45), and zircon standard GJ-1 yielded an average $^{176}Hf/^{177}Hf$ value of 0.282013 ± 0.000005 (MSWD = 0.34). Additional analytical metadata for U-Pb and Lu-Hf analyses can be found in the supporting information (Text S1 [see footnote 1]).

Data Compilation

Zircon U-Pb age distributions incorporated data from Phanerozoic-aged grains from river sands, sandstones, and metasedimentary rocks in Argentina (Figs. 6A and 6B; Cristofolini et al., 2012; Capaldi et al., 2017, 2020; this study) and beach sands, river sands, and metasedimentary rocks in Chile (Figs. 6A and 6B; Table S8; Willner et al., 2008; Pepper et al., 2016). Felsic to intermediate melt compositions recorded by zircon Th/U ratios were compared with a synthesis of new detrital zircon Hf isotopic results (Table S7), previously published detrital zircon Hf results (Fig. 6C; Willner et al., 2008; Pepper et al., 2016; Otamendi et al., 2017), and zircon Hf isotopic results from bedrock samples (Fig. 6C; Table S9; Dahlquist et al., 2013, 2016, 2018; Hervé et al., 2014; Jones et al., 2015; Otamendi et al., 2017; Rapela et al., 2018). The zircon U-Th-Pb and Hf isotopic data sets were integrated with an extensive compilation of bedrock geochronologic data to define temporal, spatial, and compositional variation in Phanerozoic magmatism along the western margin of South America.

Results: Temporal and Spatial Isotopic Patterns

The compiled zircon U-Pb and isotopic results from Argentina and Chile (28°S–33°S) record 550 m.y. of arc magmatism with the following age modes and associated isotopic signatures (Figs. 7A and 7B): (1) a gradual decrease in the relative abundance of Ediacaran–early Devonian (550–385 Ma) ages coincident with low εHf values (–4 to –2 mean values) and Th/U ratios (0.48–0.65 mean values); (2) persistent Late Devonian–Triassic (380–208 Ma) age components characterized by a positive isotopic shift in both εHf values (+5 units) and Th/U ratios (+0.3); and (3) Jurassic–Neogene (190–4 Ma) ages

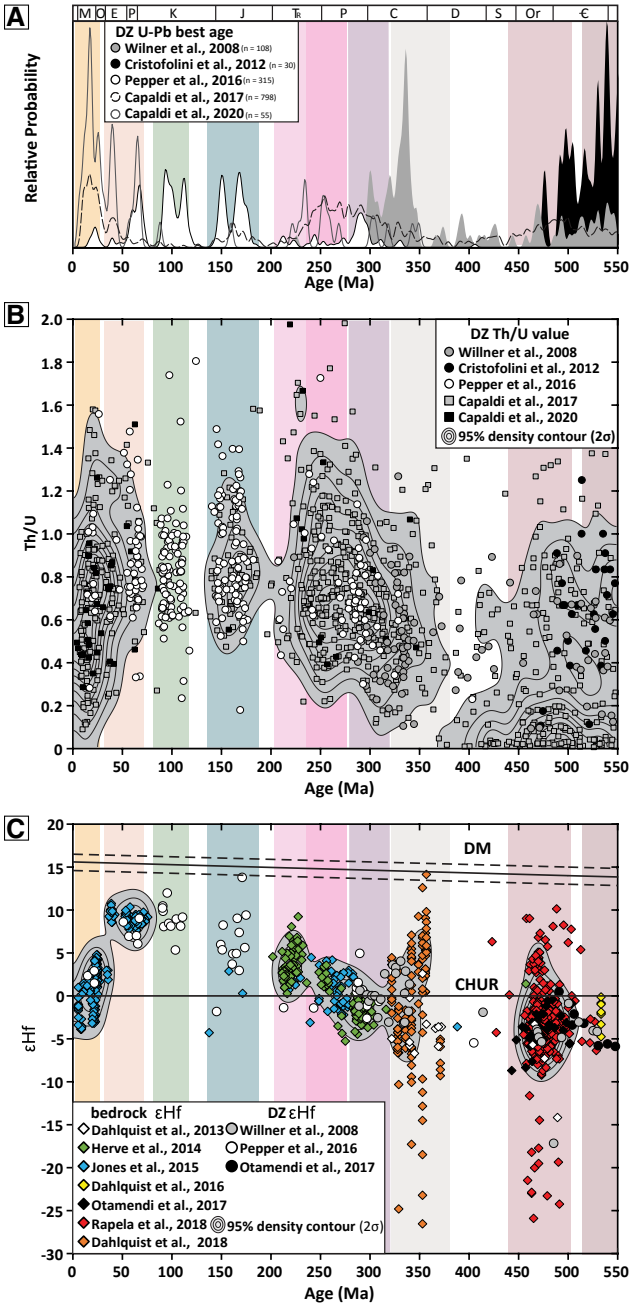

Figure 6. Compilation of published detrital zircon (DZ) and bedrock radiogenic isotopic data from Argentina and Chile. (A) Detrital zircon U-Pb age distributions from Argentina retroarc and Chile forearc samples as kernel density estimates (equal-area, 2 m.y. set kernel bandwidths). (B) Two-dimensional (2-D) view of combined U-Pb age–Th/U results plotted as bivariate kernel density estimates for zircons (10 m.y. and 0.1 Th/U unit set kernel bandwidths). (C) Two-dimensional (2-D) view of combined U-Pb age–εHf results plotted as bivariate kernel density estimates for zircons younger than 550 Ma (10 m.y. and 2ε unit set kernel bandwidths) from Argentina retroarc and Chile forearc samples. DM—depleted mantle, CHUR—chondritic uniform reservoir. Intensity contour plot represents 95% of the maximum intensity. Date were plotted using IsoplotR software (Vermeesch, 2018) and Hafnium Plotter software (Sundell et al., 2019). Є—Cambrian; Or—Ordovician; S—Silurian; D—Devonian; C—Carboniferous; P—Permian; Tr—Triassic; J—Jurassic; K—Cretaceous; P—Paleocene; E—Eocene; O—Oligocene; M—Miocene.

that display recurring 20–30 m.y. high-flux events and lulls in zircon age abundances during continental arc magmatism and exhibit a negative isotopic shift in both εHf values (–5 units) and Th/U ratios (–0.2) around 25 Ma. General agreement between the detrital zircon and bedrock compilation for central Argentina and Chile indicates that U-Th-Pb and Lu-Hf data derived from detrital samples provide a powerful tool for interrogating long-lived records of magmatism and effectively fill potential data gaps in the available bedrock record. Compiled detrital zircon U-Th-Pb–εHf results are summarized in Table 1.

Time-space variations in magmatism were tracked using a compilation of Phanerozoic igneous bedrock radiometric ages (Fig. 7C; Pilger, 2018). Ediacaran–Early Devonian (550–385 Ma) magmatism occurred principally in the eastern (68°W–63°W) regions of the present-day Sierras Pampeanas and jumped westward with sequential terrane accretion events. Late Devonian–Triassic (380–208 Ma) magmatism was focused at 70.5°W–70°W, along the present-day Principal Cordillera, with the exception of an eastward expansion of magmatic activity during Permian–Triassic (280–238 Ma) time. Jurassic–Neogene (190–4 Ma) magmatism recorded a gradual eastward advance involving Jurassic to Paleocene–Eocene volcanism in the Coastal Cordillera (71°W–70°W) followed by a rapid eastward shift during the Oligocene–Pliocene.

PHANEROZOIC TECTONIC RECONSTRUCTION

Trends in magmatic activity, zircon geochemical signatures, and locations of arc magmatism were integrated to reconstruct the geodynamic evolution of the plate margin (Figs. 7 and 8). Major tectonic phases included: (1) Ediacaran–Devonian terrane accretion, (2) Carboniferous to Triassic Gondwanan subduction, and (3) Mesozoic–Cenozoic Andean orogenesis.

Paleozoic Terrane Accretion

Zircon geochemical signatures in the eastern craton region correspond with Cambrian–Ordovician

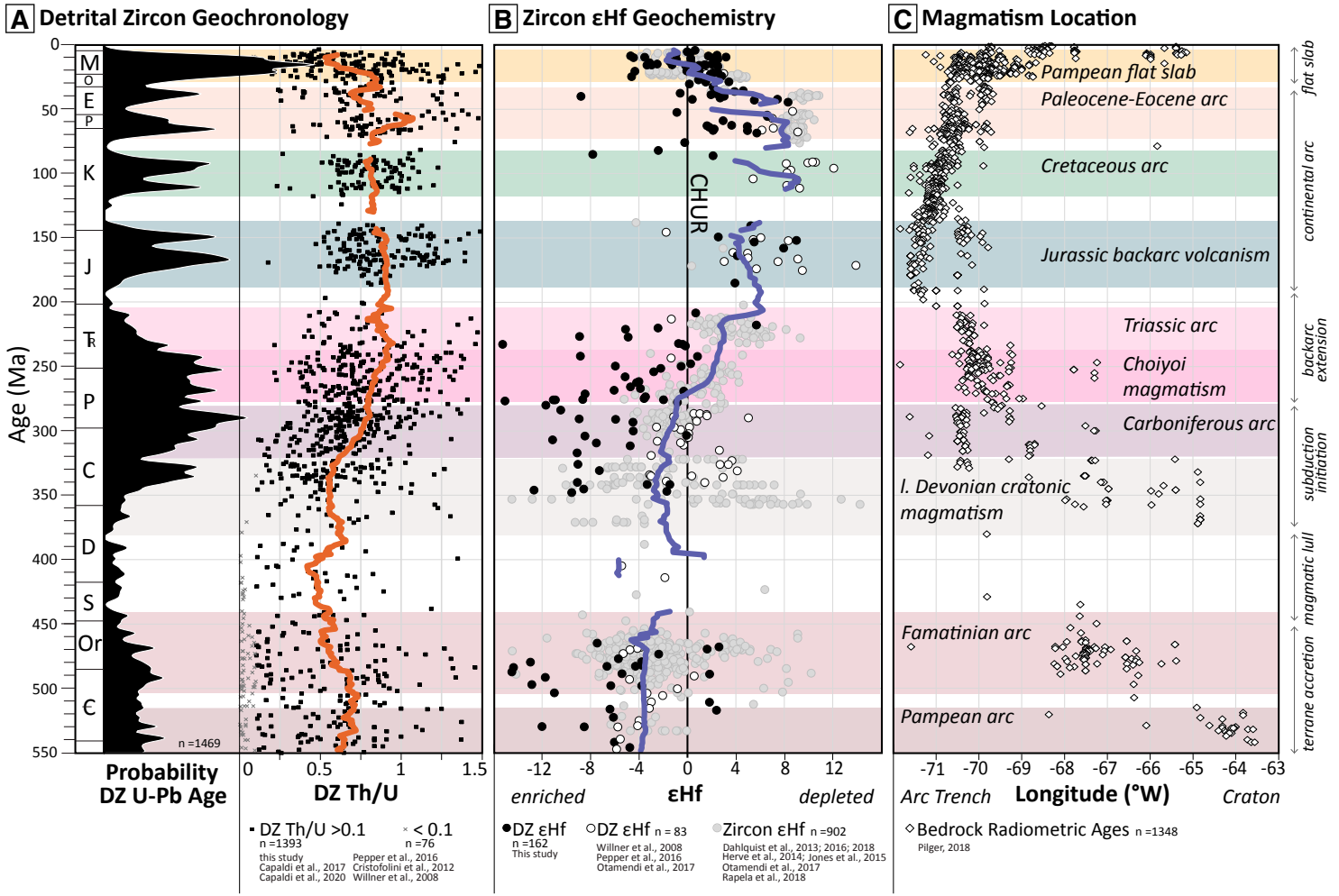

Figure 7. Comparisons of Phanerozoic temporal magmatic, compositional, and spatial trends for the western South American margin (28.5°S to 33°S); see Figure 1 for sample locations. (A) Detrital zircon U-Pb age distributions of Phanerozoic samples (550–0 Ma) with a kernel density estimate bandwidth of 2 m.y. and corresponding zircon Th/U ratios. (B) Synthesis of detrital and bedrock zircon Hf isotopic results in εHf notation. Colored trend lines are 2 m.y. moving average windows. CHUR—chondritic uniform reservoir. (C) Summary of bedrock radiometric ages showing the time-space variations by sample longitude (°W) location (Pilger, 2018), where 1° change in longitude is ~95 km. Colored horizontal bars highlight the duration of regional tectonic events and corresponding lithosphere-scale cross-sections in Figure 8. See Figure 6 caption for time scale abbreviations.

TABLE 1. ZIRCON DATA COMPILATION, SOUTHERN CENTRAL ANDES

Age group	Age min (Ma)	Age max (Ma)	Th/U min	Th/U max	Th/U mean	εHf min	εHf max	εHf mean
Oligocene–Pliocene	4	30	0.10	2.02	0.71	–25	5	1
Cretaceous–Eocene	33	74	0.24	2.13	0.84	–26	11	7
Cretaceous	82	118	0.23	1.74	0.82	–8	12	7
Jurassic	140	190	0.18	2.04	0.91	–2	14	6
Triassic	208	238	0.22	2.05	0.89	–15	9	3
Permian–Triassic	238	280	0.22	1.98	0.81	–15	5	–1
Carboniferous–Permian	281	320	0.12	1.57	0.67	–11	5	–2
Devonian–Carboniferous	321	380	0.10	1.31	0.58	–35	14	–2
Silurian–Devonian	385	435	0.11	1.53	0.48	–6	6	–2
Ordovician	440	505	0.10	2.43	0.65	–26	10	–4
Cambrian	515	550	0.11	2.00	0.64	–12	5	–4

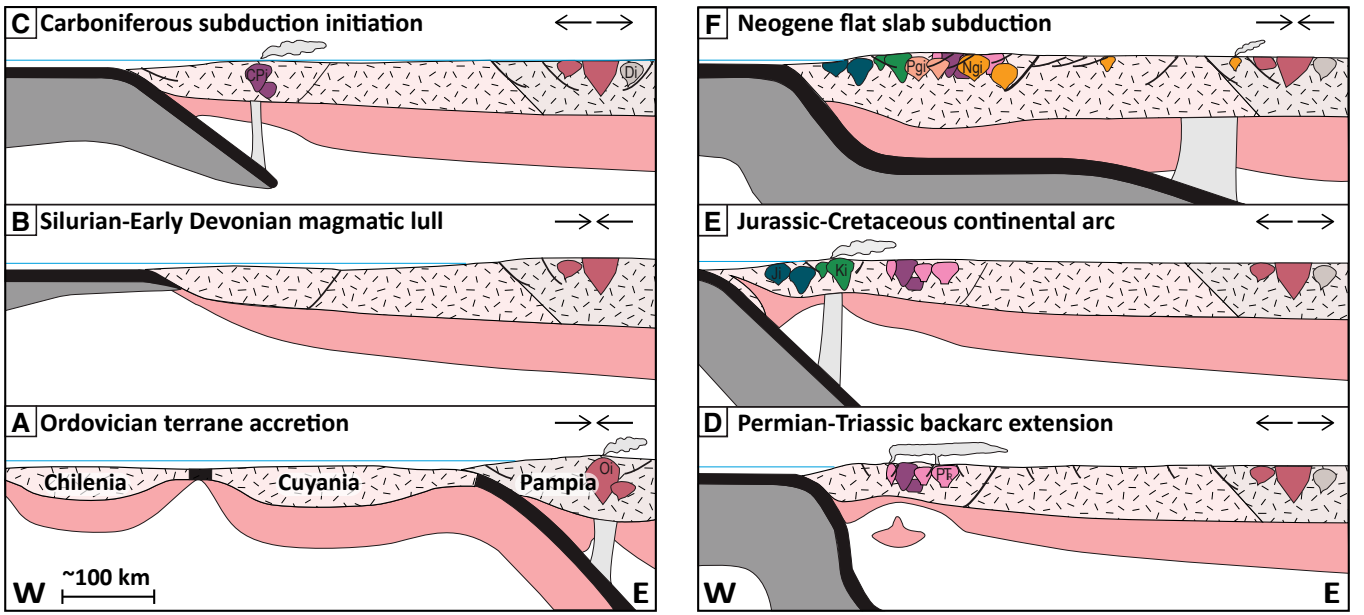

Figure 8. Tectonic models for key Phanerozoic events along the western South American margin. (A) Cambrian–Ordovician terrane accretion. (B) Silurian–Early Devonian magmatic lull. (C) Carboniferous subduction initiation. (D) Permian–Triassic backarc extension. (E) Jurassic–Paleocene continental arc. (F) Neogene flat slab subduction. See Figure 1 for abbreviations.

(550–440 Ma) igneous and metamorphic belts that exhibit evolved magmatic patterns and metamorphic zircon growth, which correspond to the collision of Laurentian continental blocks with the Gondwanan margin of South America (Fig. 8A; Schwartz et al., 2008; Ducea et al., 2010; Rapela et al., 2016). The relatively negative εHf isotopic values are indicative of evolved magma generation through thick Mesoproterozoic continental crust, a pattern consistent with shortening and crustal thickening during Pampean (555–515 Ma) and Famatinian (460–440 Ma) orogenesis (Coira et al., 1982; Astini et al., 1995; Casquet et al., 2001; Ramos, 2004, 2010; Schwartz et al., 2008; Charrier et al., 2015; Augustsson et al., 2016). The significant ~300 km westward shift in early Paleozoic magmatism over ~30 m.y. is compatible with subduction migration following these terrane accretion events. Diminished detrital zircon U-Pb age components at ca. 440 Ma suggest arc cessation occurred immediately following accretion of the Cuyania terrane (Fig. 8A; Thomas et al., 2015; Rapela et al., 2016; Martin et al., 2019).

Low relative proportions of Silurian–Devonian (435–385 Ma) zircon grains are associated with a magmatic lull and formation of metamorphic zircon supported by relatively enriched εHf values and low (<0.1) Th/U ratios. These low-abundance zircons may record magmatic quiescence related to continued collisional orogenesis linked to possible terrane accretion, prolonged flat slab subduction, or development of a passive or transform margin (Fig. 8B; Ramos et al., 1984; Sims et al., 1998; Bahlburg et al., 2009; Giambiagi et al., 2014; Cawood, 2005; Ramos, 2009; Rapalini, 2018; Dahlquist et al., 2018). We favor a model of continued shortening during final amalgamation of terrane accretion due to the lack of subduction-related magmatism and predominance of metamorphic zircon.

Devonian–Permian Subduction Initiation

The Late Devonian–early Carboniferous geodynamic setting of the pre-Andean margin of Gondwana is unresolved, with some arguing for a passive-margin setting (Bahlburg et al., 2009; Herve et al., 2013, 2014) and others suggesting postcollisional magmatism related to terrane accretion (Willner et al., 2012). The mid-Paleozoic lull in igneous activity was followed by Late Devonian magmatism located throughout the Sierras Pampeanas provinces (Fig. 7). Late Devonian to early Carboniferous (380–320 Ma) magmatism was expressed as widely distributed (>500 km) granitic plutons emplaced during extensional conditions (Fig. 8C; Dahlquist et al., 2013; Moreno et al., 2020). This is consistent with isotopically enriched magmatism with a mean εHf value of –2 and mean Th/U ratio of 0.6, linked to magmas derived from lithospheric mantle and recycled continental crustal sources with possible upper-crustal contamination (Dahlquist et al., 2013). This type of magmatism has been attributed to incipient subduction during slab rollback and upper-plate extension (Alasino et al., 2012; Dahlquist et al., 2013; del Rey et al., 2016). We interpret late Paleozoic (re)establishment of a convergent subduction margin along the western edge of South America on the basis of Carboniferous magmatism (Fig. 8C). The proposed initiation of subduction was associated with westward (trenchward) retreat of magmatic activity, and this is supported by petrographic and metamorphic age relationships within the Paleozoic forearc subduction complex that record convergence initiating between ca. 343 and 310 Ma (Willner et al., 2008, 2012). Carboniferous magmatism was interrupted by the punctuated Gondwanide compressional event (284–270 Ma), which was recorded by intense folding and thrusting along a NW-NNW–trending orogen in the Argentinian Frontal Cordillera and San Rafael uplift further south (Ramos et al., 1986; Llambias and Sato, 1995; Franzese and Spalletti, 2001; Kleiman and Japas, 2009; Ramos and Folguera, 2009; Giambiagi et al., 2014; del Rey et al., 2016).

Permian–Triassic Continental Breakup

The spatially extensive Permian–Triassic magmatic trend does not reflect a decrease in slab angle and associated magmatic arc widening; rather, it is exemplified by the Choiyoi igneous complex, a suite of intrusive and extrusive igneous rocks associated with an extensive ignimbrite flareup along the southwestern margin of Gondwana (Fig. 8D; Kay et al., 1987; Llambías et al., 2003; Nelson and Cottle, 2019). The Choiyoi igneous complex progressed from granitic/dacitic magmas during convergent arc magmatism (290–265 Ma) to intermediate or bimodal compositions during extensional magmatism (265–240 Ma) as the upper plate transitioned to postorogenic collapse (Mpodozis and Kay, 1992; Kleiman and Japas, 2009). Mechanisms that would have generated spatially broad, trenchward-retreating volcanism include subducting slab rollback and lithosphere delamination beneath Gondwana, with resulting crustal thinning and upper-plate extension driving ignimbrite flareup phases (Fig. 7D; Kay et al., 1987; Pankhurst et al., 2006; Nelson and Cottle, 2019).

Triassic (238–208 Ma) zircons record positive mean εHf values and a systematic increase in Th/U ratios to 0.9, suggestive of increased depleted components related to asthenospheric upwelling triggered by extensional thinning. The petrography, geochemistry, and isotopic composition of Triassic volcanic rocks show progressive changes over time yet indicate dominant subduction-related characteristics since the Carboniferous (Vásquez et al., 2011; Poma et al., 2014; del Rey et al., 2016; Coloma et al., 2017; Oliveros et al., 2018; González et al., 2018). In this manner, a combination of postorogenic collapse and backarc extension during slab rollback marked the onset of a principally extensional to neutral tectonic regime that characterized much of western South America during the Mesozoic (Fig. 8E; Rossel et al., 2013; Oliveros et al., 2018).

Mesozoic–Cenozoic Andean Margin

Reconstructed subduction angle estimates from the Late Triassic to present can address potential temporal linkages between variations in the subducted plate and associated magmatic geochemical signatures and the tectonic setting (Fig. 9). The distribution of arc magmatism reveals several shifts in subduction angle estimates that broadly decrease throughout the Mesozoic–Cenozoic (Fig. 9A), which are paralleled by a similar trend

in decreasing zircon isotopic signatures (Fig. 9B). During the 230 m.y. span of Triassic to present arc magmatism, 8 high-flux events are recorded by zircon U-Pb age peaks at 230–204, 184–160, 156–136, 118–105, 102–82, 74–52, 46–32, and 28–4 Ma, which typically span ~10–25 m.y. and are interrupted by magmatic lulls that decrease in duration through time from Jurassic (20 m.y.) to Miocene (<5 m.y.). Increased arc frequency appears to correspond with a decrease in subduction angle and more negative εHf magmatic signatures.

Compositional and temporal patterns in arc magmatism were compared to the retroarc basin record to highlight how observed variations in magmatism temporally correlate with periods of Andean extension and orogenesis. A synthesis of Mesozoic–Cenozoic sediment accumulation histories for Andean extensional and compressional retroarc basins records the onset of major phases of subsidence and temporal shifts in accumulation, which provide constraints for the onset and pace of extension, contractional orogenesis, and tectonic subsidence (Fig. 9C; Kent et al., 2014; Fosdick et al., 2017; Mackaman-Lofland et al., 2019). Relationships among Andean subduction, arc magmatism, and retroarc basin evolution are related to first-order plate kinematics of the South American plate

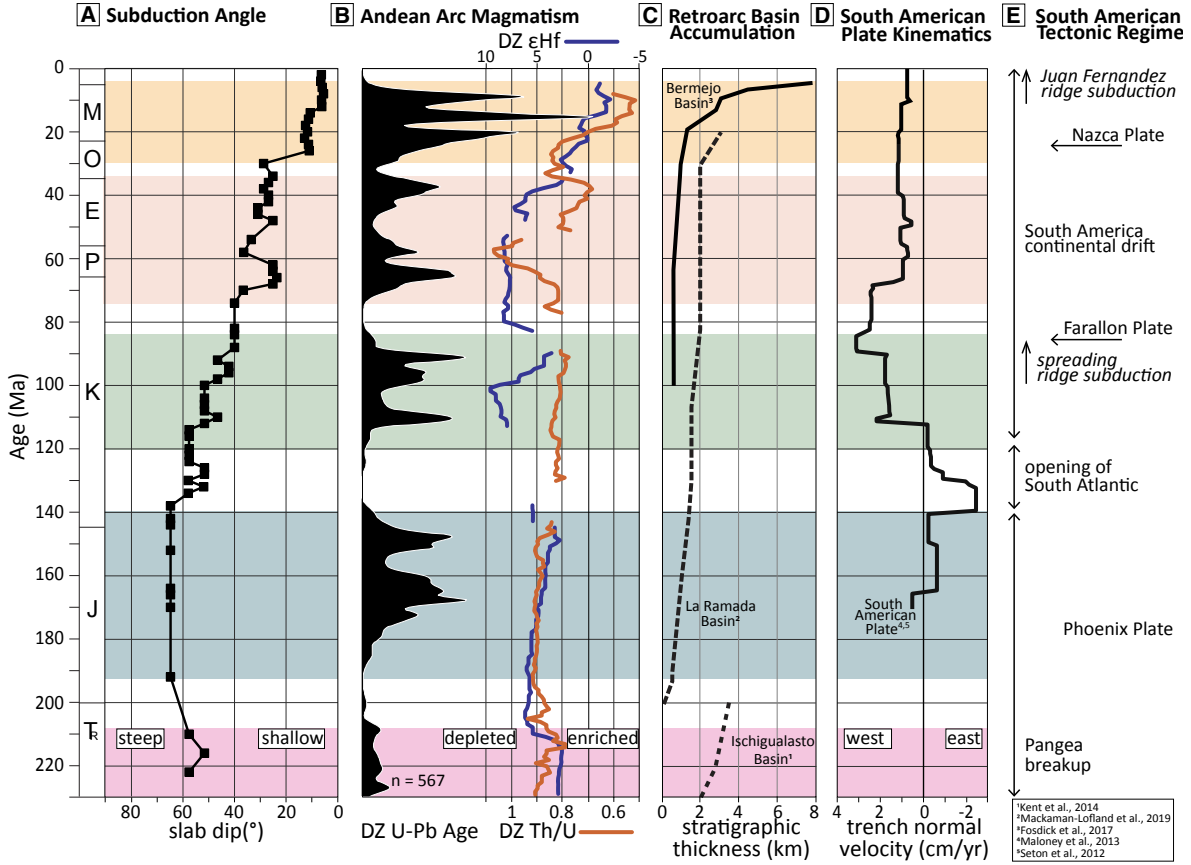

Figure 9. Plot comparing Mesozoic and Cenozoic: (A) calculated subduction angle, (B) detrital zircon (DZ) U-Pb geochronology age distributions displaying Andean magmatism and mean U/Th ratios (orange line) and εHf values (blue line), (C) retroarc basin accumulation plot, (D) South American plate velocity model tracking changes to trench-normal velocities, and (E) South American plate-tectonic regimes. See Figure 4 caption for time scale abbreviations.

(Fig. 9D). We show global plate kinematic reconstructions for varied oceanic plates of the Pacific Ocean basin relative to a fixed South American plate from 170 Ma to present alongside our data to emphasize the role played by plate dynamics in Andean subduction (Seton et al., 2012; Maloney et al., 2013).

Triassic to Jurassic

Triassic to Jurassic magmatism was coeval with relatively high subduction angle (55°–65° slab dip), which reflects a prolonged phase of slab-rollback and crustal extension (Fig. 9A). Zircons recorded consistently positive ~5 mean εHf values and >0.8 mean Th/U values, reflecting phases of juvenile arc and associated backarc magmatism indicative of slab-dehydration melting in the upper mantle (Fig. 9B; Vergara et al., 1995; Charrier et al., 2002, 2015; Rossel et al., 2013; Balgord, 2017). Time versus thickness diagrams display initial Triassic sediment accumulation curves that show progressively diminished sedimentation rates from 230–200 m.y. to 200–100 m.y. (Fig. 9C). This concave-upward sediment accumulation pattern is attributed to fault-controlled and subsequent thermal subsidence in the Triassic Cuyo and Ischigualasto basin systems (Ramos and Kay, 1991; Currie et al., 2009; Barredo, 2012; Kent et al., 2014) and Jurassic La Ramada backarc basin (Alvarez and Ramos, 1999; Oliveros et al., 2012; Mackaman-Lofland et al., 2019). The trench-normal absolute velocity of the South American plate reveals initial Triassic to Jurassic east-directed motion away from the trench, coeval with the breakup of Pangea (Fig. 9D; Storey, 1995; Ramos, 2009).

Cretaceous to Paleogene

An Early Cretaceous (ca. 140–120 Ma) lull in Andean arc magmatism was associated with intra-arc transtensional faulting along the Atacama fault system in Chile (Seymour et al., 2020). Early Mesozoic extensional basin subsidence was followed by Early Cretaceous neutral stress conditions and protracted thermal subsidence (Horton, 2018b; Mackaman-Lofland et al., 2019). Cretaceous (118–82 Ma) magmatism along the Coastal Cordillera of Chile records decreased subduction angle from 55° to 40° and isotopic decrease in εHf composition (Fig. 9B) that was coeval with a Late Cretaceous phase of contractional deformation (Parada et al., 2005; Litvak et al., 2007; Charrier et al., 2015; Horton et al., 2016; Mackaman-Lofland et al., 2019). Basin thickness versus time profiles exhibit a Late Cretaceous inflection around 105 Ma that corresponds with a convex-upward sediment accumulation curve in the La Ramada basin and initiation of deposition in the distal Bermejo foreland (Fig. 9C). Accelerated accumulation of sediment defines the onset of initial Andean shortening and deposition in a proximal Andean foreland basin (Fosdick et al., 2017; Mackaman-Lofland et al., 2019). A major shift in absolute plate motion at 110–90 Ma suggests the South American plate transitioned from a net retreating subduction system during Jurassic–Early Cretaceous time (including initial opening of the South Atlantic Ocean) to a net advancing system during the Late Cretaceous, contemporaneous with early Andean shortening (Figs. 8E and 9D; Torsvik et al., 2009; Seton et al., 2012; Horton, 2018a).

A latest Cretaceous magmatic lull (82–74 Ma) was associated with transpressional faulting in the Coastal Cordillera (Taylor et al., 1998). Paleogene subduction angle remained relatively consistent at 25°–35° eastward dip with minimal deformation recorded in the upper plate (Fig. 9A). Latest Cretaceous–Eocene (74–32 Ma) increased εHf and Th/U values are indicative of magmatism produced by slab-derived fluids and enhanced melting in the mantle wedge (Fig. 9B; Litvak and Poma, 2010; Jones et al., 2016). Subsequent Eocene to Oligocene volcanism records diminished εHf and Th/U values, suggestive of mantle wedge enrichment due to increased crustal assimilation or subducted sediment associated with increased forearc erosion (Kay and Mpodozis, 2002; Kay et al., 2005; Litvak et al., 2007; Jones et al., 2016; Lossada et al., 2017). The latest Cretaceous to early Paleogene interval was characterized by a depositional hiatus in the proximal La Ramada basin and slow accumulation in distal retroarc regions, which may reflect negligible shortening and orogenic loading during a neutral stress regime (Fig. 9C; Horton and Fuentes, 2016; Mackaman-Lofland et al., 2019). Reduced westward motion of the South America plate characterized the Paleogene, which is compatible with relatively diminished shortening (Fig. 9D).

Oligocene–Pliocene

Zircon age populations for the Oligocene–Pliocene (32–4 Ma) record broadening of the magmatic arc and an isotopic decrease in both zircon εHf and Th/U ratios that corresponds with the shallowing of the subduction angle (Figs. 8F and 9A; Kay and Mpodozis, 2002; Jones et al., 2016). Oligocene volcanic rocks yielded geochemical signatures characteristic of partial melting of mantle wedge material (Kay and Abbruzzi, 1996; Jones et al., 2016; Litvak et al., 2018) and were associated with intra-arc oblique faulting (Piquer et al., 2017; Mosolf et al., 2019; Mackaman-Lofland et al., 2019). Middle Miocene arc volcanism was defined by isotopic signatures indicative of crustal thickening (>50 km; Kay et al., 1991; Jones et al., 2015). Arc broadening, flareup, and crustal thickening were synchronous with shortening and erosion along the Frontal Cordillera and early foreland basin development across the retroarc (Fosdick et al., 2017; Buelow et al., 2018; Pinto et al., 2018; Mackaman-Lofland et al., 2020). The rapid thickening of the Andean crust and relative advancement of the arc in the late Miocene produced more evolved arc magmatism as the flat slab propagated eastward post–12 Ma (Fig. 9B; Kay and Mpodozis, 2002; Allmendinger and Judge, 2014; Jones et al., 2016; Capaldi et al., 2020). Following continued flattening of the subducted slab, major arc activity within the Principal Cordillera ceased by ca. 5 Ma, and diffuse volcanic centers across the Precordillera and Sierras Pampeanas continued until ca. 2 Ma (Kay and Abbruzzi, 1996; Ramos and Folguera, 2009). The main phase of Andean orogenesis corresponded to rapid Neogene sedimentation, where 3–8-km-thick fill denotes major flexural subsidence in foreland settings (Fig. 9C; Jordan et al., 1993; Fosdick et al., 2015).

The Pliocene to Quaternary crustal response to flat slab subduction involved a shift in deformation from a thin-skinned thrust belt to series of basement-involved foreland uplifts and eastward progression of coarse-grained deposystems within the broken foreland basin system (Capaldi et al., 2020). Initiation of shortening in the early Miocene may have been associated with a shift in Nazca plate motion, leading to enhanced trench-normal convergence, potential shallowing of subduction angle, and initial subduction of the Juan Fernandez Ridge, which rapidly migrated southward (~20 cm/yr) along the South American margin (Fig. 9D; Yáñez et al., 2001; Martinod et al., 2010). Nazca plate reconstructions indicate that late Miocene (ca. 11 Ma) arrival of the relatively thick, younger oceanic crust of the Juan Fernandez Ridge to the Chile Trench at 31°S induced Pampean flat slab subduction (Fig. 9E; Pilger, 1981, 1984; Kay et al., 1991; Yáñez et al., 2001; Ranero et al., 2006). Neogene magmatism displays isotopically enriched signatures that correspond with subduction angle decrease, crustal thickening, and magmatism that advanced toward the craton and intruded thicker continental lithosphere.

DISCUSSION

Integration of Phanerozoic zircon U-Pb age distributions, U-Th and Lu-Hf geochemical data, and the spatial distribution of magmatism provides new insights into the potential drivers of the magmatic compositional variability along the South American margin. Here, we (1) discuss spatial trends in zircon isotopic signals with respect to variable crustal composition, (2) propose variations in subduction angle as the main driving mechanism for Mesozoic–Cenozoic magmatic arc migration, and (3) evaluate our results in the context of competing Cordilleran models for the South American margin.

Spatial Trends in Magmatism Composition

The South American crust at 28°S–33°S contains north-south–trending terranes with variable composition that may have induced a spatial control on crustal geochemical signatures inherited by subsequent Andean tectono-magmatic regimes. Coupled zircon geochemical data and correlative bedrock locations exhibit a similar spatial pattern in both U-Th-Pb and Lu-Hf systems, such that magmatic activity in the western Principal Cordillera and Coastal Cordillera was associated with higher zircon isotopic values, in contrast with relatively lower values in eastern magmatic sources (Fig. 10). The parallel trends in zircon geochemistry appear to follow the proposed location of the suture between the Chilenia and Cuyania terranes at ~69°W. West of 69°W, Mesozoic to Cenozoic zircon εHf averages are mostly >0, and the Th/U ratio averages exceed ~0.75 (Fig. 10). Trenchward retreat of the magmatic arc commenced after extensive Choiyoi magmatism,

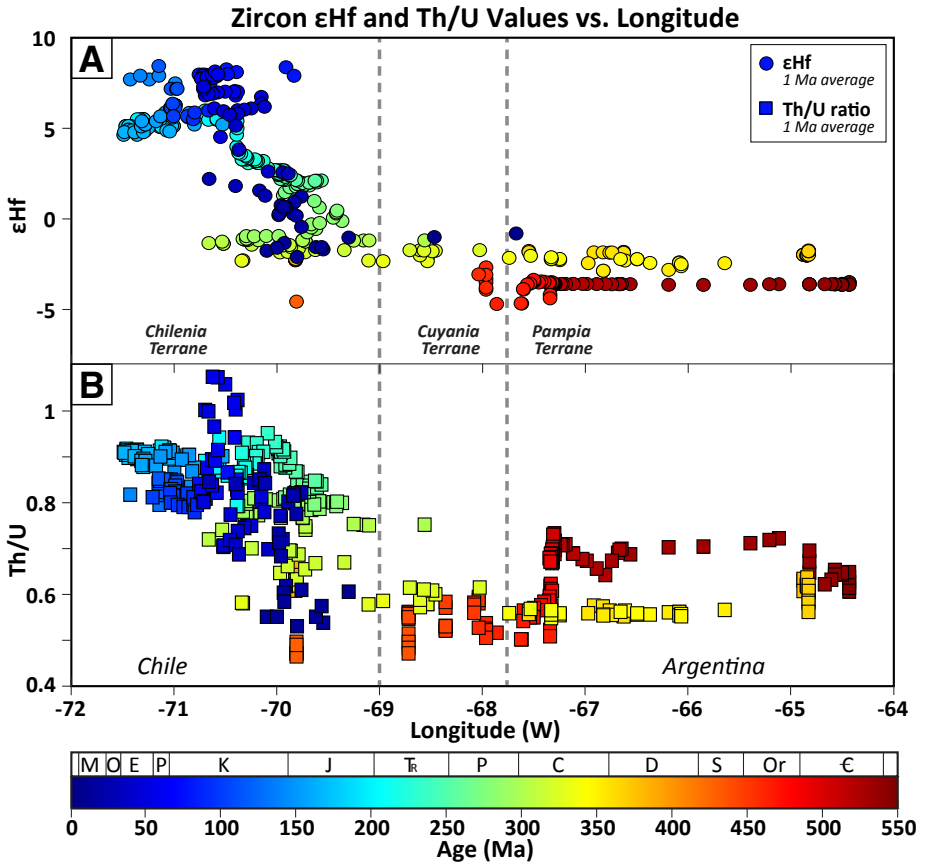

Figure 10. Spatial and temporal trends in Phanerozoic radiogenic isotopic values from Argentina and Chile (28.5°S to 33°S). (A) Averaged zircon εHf values and (B) zircon Th/U values were calculated using a 1 m.y. average moving window for Phanerozoic (0–550 Ma) isotopic values (Figs. 7A and 7B; Table S5 [see text footnote 1]) and compared against spatial trends using 1 m.y. average moving window for Phanerozoic (0–550 Ma) radiogenic age locations (Fig. 7C). Color map tracks the age of the magmatism. Spatial trends show that composition of magmatism becomes more isotopically enriched (–εHf) with lower Th/U ratio eastward of the trench. See Figure 7 caption for time scale abbreviations.

with reduced crustal assimilation during magma ascent through thinner, possibly juvenile crust and melting of upwelling, depleted asthenosphere of the Chilenia terrane. East of 69°W, zircon εHf values range between –5 and –2 with Th/U ratios less than 0.7 (Fig. 10). Magmatism farther from the trench is characterized by more enriched radiogenic isotopic signatures due to the composition of eastern Precambrian terranes (i.e., Cuyania and Sierras Pampeanas). These trends highlight a spatial relationship that reflects contrasting source regions, with asthenospheric (juvenile) compositions near the trench and more lithospheric (evolved) contributions toward the craton (Hildreth and Moorbath, 1988; Pepper et al., 2016; Chapman et al., 2017). Thus, inboard arc migration produces a shift to more enriched compositions (Chapman and Ducea, 2019). Variation in subduction angle is a potential mechanism that affects Cordilleran arc migration, arc widening, and shifts in isotopic composition.

Slab Angle Drives Arc Migration

Spatial, temporal, and compositional changes in continental arc magmatism along the Andean margin are shown to be related to variations in subduction angle (Ramos et al., 2002). Here, we compared Mesozoic to Cenozoic (220–0 Ma) slab dip estimates with time-averaged εHf and Th/U zircon results (Fig. 9), which show decreasing (enriched) magma compositions with increasing arc width (Fig. 11A) and decreasing slab dip (Fig. 11B). Narrow (<75 km) magmatic arcs correspond to steep (>50°) subduction, with elevated εHf and Th/U zircon values. In contrast, wider (>300 km) magmatic arcs correlate with low-angle (<15°) subduction and diminished εHf and Th/U zircon values (Fig. 11). Moderate subduction angles (~20°–50°) generally show a decrease in εHf and Th/U zircon values with decrease in slab dip, albeit with greater variability. Others have demonstrated that arc migration driven by an increase in subduction rates and forearc erosion may also impart a more enriched geochemical signature in Andean magmatism (e.g., Kay et al., 2005; Stern, 2011). However, arc migration driven exclusively by subduction erosion cannot account for the observed range in preserved widths for the Mesozoic–Cenozoic Andean arc. Here, we suggest that more evolved magma compositions are associated with a decrease in slab dip that induces cratonward arc migration with enhanced contributions from Precambrian lithosphere, whereas slab steepening and arc retreat involve magmatic sources from depleted asthenospheric mantle of the accreted Chilenia terrane.

Implications for Cordilleran Tectonics

We compared the spatial, temporal, and compositional variations in the magmatic history of

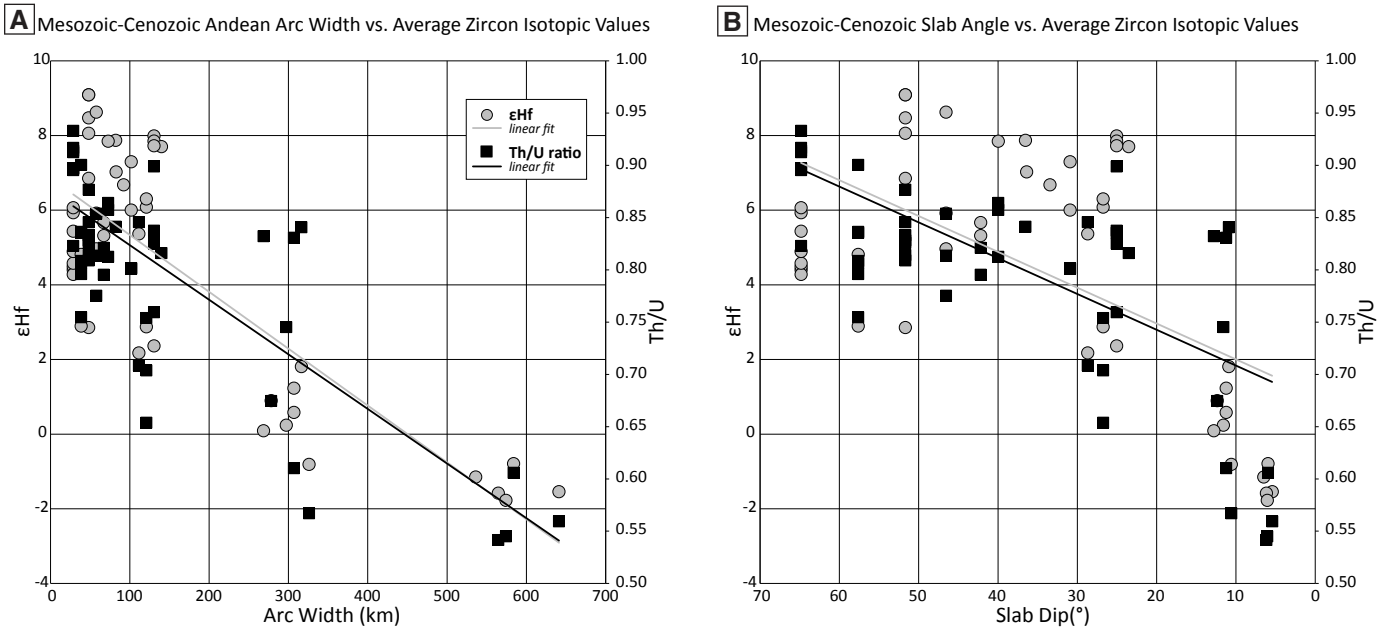

Figure 11. Comparisons of Mesozoic–Cenozoic Andean arc width, subduction angle, and zircon composition along Argentina and Chile (28.5°S to 33°S). (A) Andean arc width relative to zircon εHf and Th/U values (Table S5 [see text footnote 1]). (B) Subduction angle relative to zircon εHf and Th/U values (Table S5 [see text footnote 1]).

the southern Central Andes with numerous geodynamic, tectonic, and autogenic Cordilleran models to better understand the processes driving Andean orogenesis and subduction-related magmatism.

Recent geodynamic models predict that variations in upper-plate deformation are a function of the subducted plate interacting with and anchoring into the lower mantle (Husson et al., 2012; Faccenna et al., 2017; Schellart, 2017; Chen et al., 2019; Spencer et al., 2019). During incipient subduction, these models predict viscous coupling between the retreating slab and the upper mantle that induces a return flow that drags against the trench-proximal overriding plate toward the retreating subduction zone, inducing surface extension (Schellart et al., 2007; Husson et al., 2012; Schellart, 2017). Anchoring of the subducted slab in the lower mantle generates large-scale mantle flow that induces basal drag along the overriding plate toward the trench, which then drives orogenesis progressively on short 10–20 m.y. (Faccenna et al., 2017; Chen et al., 2019) to longer 100 m.y. (Schellart, 2017) time scales. In the southern Central Andes, the increase in juvenile magmatic sources and extensional basin development during Carboniferous subduction initiation and trenchward arc retreat (Figs. 7 and 8C) support the upper-mantle convection and slab retreat geodynamic model. Carboniferous subduction initiation was followed by the punctuated Gondwanide compressional event, potentially driven by slab anchoring and increased plate convergence. However, these geodynamic models predict subduction initiation in the Jurassic or Cretaceous followed by slab anchoring over 10–20 m.y., which is at odds with the magmatic record in the southern Central Andes that preserves a clear Carboniferous subduction initiation event. Longer subduction histories (~300 m.y.) along the South American margin require reevaluations of the timing of subduction initiation and/or reinitiation, which is critical to assessing when slab anchoring and subsequent orogenesis are predicted to occur in Cordilleran systems.

One class of tectonic models relates the degree of mechanical coupling between the overriding and downgoing plates to associated tectonic regimes operating during decoupled, neutral, and coupled subduction (Jarrard, 1986; Heuret and Lallemand, 2005; Martinod et al., 2010; Ramos, 2009; Horton, 2018a, 2018b). Subduction angle, in particular, has been interpreted to modulate overriding plate processes, such that high subduction angle and slab rollback settings, where overriding plate motion is away from the subduction trench, manifest as a retreating subduction zone, trenchward arc migration, crustal thinning, and extensional basin development (Royden, 1993). In the southern Central Andes, Triassic–Jurassic juvenile magmatism indicates trenchward arc retreat and associated slab steepening that occurred coeval with a phase of backarc extension and magmatism, which may reflect a phase of decoupled subduction (Fig. 9). The protracted phase of Cretaceous and Paleogene subduction exhibited constant arc width and relatively invariant radiogenic isotopic values that are consistent with a Cordilleran system that was neither contractional nor extensional; rather, the boundary conditions reflect neutral plate coupling (Horton and Fuentes, 2016; Mackaman-Lofland et al., 2019). The Neogene decrease in slab dip angle was coeval with retroarc crustal thickening and widening of arc magmatism toward the foreland region (Ramos et al., 2002; Haschke et al., 2006; Capaldi et al., 2020). The predicted increase in mechanical coupling along the subduction interface would have been related to the relative advance of the subducting slab toward the overriding plate, inducing shallowing of subduction angle (Schellart, 2017, 2020). Additionally, the accelerated relative convergence following the Jurassic to Cretaceous opening of the South Atlantic Ocean and far-field effects from the subduction of positively buoyant oceanic lithosphere appear to be first-order drivers of coupled subduction systems (Horton, 2018a).

Segments of Cordilleran systems that sustained high (>150 km) margin-perpendicular shortening and major crustal thickening have exhibited fluctuations (possibly cyclical) in deformation and magmatism, including rapid orogenic wedge propagation, high-flux magmatic events, lithospheric removal, and extensional collapse (Haschke et al., 2002, 2006; DeCelles et al., 2009, 2015; Wells et al., 2012; Carrapa and DeCelles, 2015; Ducea et al., 2015; Anderson et al., 2018). Though Cordilleran cyclicity models do not invoke external mechanisms such as variation in subduction angle, the models do provide predictions that may explain short-term (<20 m.y.) trends observed in our zircon compositional data. Deviations from the general trend of decreasing isotopic values with decrease in subduction angle occurred at 60 Ma and 35 Ma—time points that show increases in εHf and Th/U zircon values during shallowing of the Nazca plate (Figs. 9A and 9B). Such variance in isotopic trends may indicate intra-arc processes exhibited as mixed modes of deformation consisting of possibly cyclical phases of extension or neutral stress conditions (Folguera et al., 2006; Ramos et al., 2014; Giambiagi et al., 2015), potentially driven by dynamic convective removal of lower-crustal arc roots (Currie et al., 2015). Additionally, phases of intra-arc strike-slip deformation occur during periods of subduction angle change, which may drive tectonic reorganization and structural configurations that can induce changes to the bulk compositions of the lower crust–mantle lithosphere regions beneath arcs that lead to rejuvenation of melting and high-flux events (DeCelles et al., 2015; Ducea et al., 2015).

The Phanerozoic magmatic history of the southern Central Andes preserves a strong relationship between magmatism composition and arc migration, which corresponds with subduction angle variations. Magmatic perturbations over shorter (<50 m.y.) time scale may have been associated with intra-arc deformation processes and lithospheric removal. The protracted subduction angle decrease throughout the late Paleozoic to Cenozoic may have been linked to large-scale slab anchoring and global plate kinematics associated with opening of the Atlantic Ocean. Subduction angle decrease is shown to not only drive arc migration inboard, but also enhanced plate coupling and shortening within the overriding plate. Coupled arc advance into thicker, older lithosphere and crustal thickening during orogenesis are reflected as enriched isotopic signatures and evolved magmatic phases.

CONCLUSIONS

(1) Phanerozoic detrital zircon U-Th-Pb and Hf results coupled with spatial shifts in

magmatism from the southern Central Andes (28°S–33°S) show three significant trends: (i) Ediacaran–Silurian magmatism was characterized by enriched Hf isotopic values associated with crustal thickening followed by growth of metamorphic zircons during continued accretion of exotic terranes. The spatial distribution of coeval magmatic centers further reflects westward arc migration associated with terrane accretion along the Gondwana margin. (ii) Devonian–Carboniferous zircons record enriched Hf isotopic values and inboard magmatism during subduction initiation, followed by a Permian–Triassic phase with higher, depleted isotopic signatures located along the South American margin as the upper crust extended and lower crust delaminated during slab rollback. (iii) The westernmost Jurassic arc recorded depleted magmatic signatures, which shifted to moderately juvenile as magmatism advanced progressively inboard. Neogene magmatism recorded a dramatic isotopic decrease to enriched signatures as the Nazca plate shallowed and volcanism swept inboard from the trench.

(2) Zircon U-Th-Pb and Hf analyses displayed similar spatial patterns in geochemical trends such that eastern (craton) magmatism exhibit 0 to –5 εHf and <0.7 Th/U average values, and western (Andean) magmatism exhibit 0–8 εHf and >0.7 Th/U average values. The observed spatial isotopic trends, with more radiogenically enriched magmatic signatures in the orogenic interiors, reflect the nature of the melt-source region, with greater asthenospheric (juvenile) contribution near the trench and more lithospheric contributions to magma compositions (evolved) away from the trench. Such geochemical trends highlight the spatial relationships among crustal age and composition in the eastern Precambrian terranes (i.e., Cuyania and Sierras Pampeanas) and more juvenile western terrane (Chilenia), which imparted a significant control on subsequent magmatism composition.

(3) To calibrate the relationship between arc width and slab dip, we compared Pleistocene to Holocene Andean arc volcano locations with present-day Nazca plate geometries to extract values of arc width, slab dip, and slab depth. The spatial distribution of Mesozoic–Cenozoic (220–0 Ma) igneous rocks preserves Andean magmatic arc widening and narrowing through time, from which we estimated past subduction angle. Comparisons between Mesozoic–Cenozoic slab dip calculations and time-averaged zircon results exhibited a clear trend of decreasing εHf and Th/U values, indicating enriched magma compositions, associated with arc width increase and slab dip decrease. These compositional trends in zircons reflect the spatial heterogeneity of the numerous crustal terranes affected as the arc migrated relative to the trench, and subsequent modulations in crustal thickness during orogenesis and extension along the South American margin.

ACKNOWLEDGMENTS

This research was supported by U.S. National Science Foundation grant EAR 1348031 awarded to N.R. McKenzie and B.K. Horton, a Jackson Distinguished Postdoctoral Fellowship to McKenzie, and student research grants from the Geological Society of America, American Association of Petroleum Geologists, Society for Sedimentary Geology (SEPM), and the Jackson School of Geosciences awarded to T.N. Capaldi. We thank Susanne Kay, Victor Ramos, Margo Odlum, Sarah George, Kristina Butler, Mark Helper, Emily Cooperdock, Angela Hessler, Lisa Stockli, and Jean Wong for helpful discussions. Constructive reviews by Andrea Stevens-Goddard, Joel Saylor, and Associate Editor Christopher Spencer significantly improved the manuscript.

REFERENCES CITED

Alasino, P.H., Dahlquist, J.A., Pankhurst, R.J., Galindo, C., Casquet, C., and Rapela, C.W., Larrovere, M.A., and Fanning, C.M., 2012, Early Carboniferous sub- to mid-alkaline magmatism in the Eastern Sierras Pampeanas, NW Argentina: A record of crustal growth by the incorporation of mantle-derived material in an extensional setting: Gondwana Research, v. 22, no. 3–4, p. 992–1008, https://doi.org/10.1016/j.gr.2011.12.011.

Allmendinger, R.W., and Judge, P.A., 2014, The Argentine Precordillera: A foreland thrust belt proximal to the subducted plate: Geosphere, v. 10, p. 1203–1218, https://doi.org/10.1130/GES01062.1.

Alvarado, P., Pardo, M., Gilbert, H., Miranda, S., Anderson, M., Saez, M., and Beck, S., 2009, Flat-slab subduction and crustal models for the seismically active Sierras Pampeanas region of Argentina, *in* Kay, S.M., Ramos, V.A., and Dickinson, W.R., eds., Backbone of the Americas: Shallow Subduction, Plateau Uplift, and Ridge and Terrane Collision: Geological Society of America Memoir 204, p. 261–278, https://doi.org/10.1130/2009.1204(12).

Alvarez, P.P., and Ramos, V.A., 1999, The Mercedario rift system in the Principal Cordillera of Argentina and Chile (32°SL): Journal of South American Earth Sciences, v. 12, p. 17–31, https://doi.org/10.1016/S0895-9811(99)00004-8.

Ancellin, M.A., Samaniego, P., Vlastelic, I., Nauret, F., Gannoun, A., and Hidalgo, S., 2017, Across-arc versus along-arc Sr-Nd-Pb isotope variations in the Ecuadorian volcanic arc: Geochemistry Geophysics Geosystems, v. 18, p. 1163–1188, https://doi.org/10.1002/2016GC006679.

Anderson, R.B., Long, S.P., Horton, B.K., Thomson, S.N., Calle, A.Z., and Stockli, D.F., 2018, Orogenic wedge evolution of the central Andes, Bolivia (21°S): Implications for Cordilleran cyclicity: Tectonics, v. 37, no. 10, p. 3577–3609, https://doi.org/10.1029/2018TC005132.

Astini, R.A., Benedetto, J.L., and Vaccari, N.E., 1995, The early Paleozoic evolution of the Argentine Precordillera as a Laurentian rifted, drifted, and collided terrane: A geodynamic model: Geological Society of America Bulletin, v. 107, p. 253–273, https://doi.org/10.1130/0016-7606(1995)107<0253:TEPEOT>2.3.CO;2.

Augustsson, C., Willner, A.P., Rüsing, T., Niemeyer, H., Gerdes, A., Adams, C.J., and Miller, H., 2016, The crustal evolution of South America from a zircon Hf-isotope perspective: Terra Nova, v. 28, p. 128–137, https://doi.org/10.1111/ter.12200.

Bahlburg, H., Vervoort, J.D., Du Frane, S.A., Bock, B., Augustsson, C., and Reimann, C., 2009, Timing of crust formation and recycling in accretionary orogens: Insights learned from the western margin of South America: Earth-Science Reviews, v. 97, no. 1–4, p. 215–241, https://doi.org/10.1016/j.earscirev.2009.10.006.

Balgord, E.A., 2017, Triassic to Neogene evolution of the south-central Andean arc determined by detrital zircon U-Pb and Hf analysis of Neuquen Basin strata, central Argentina (34°S–40°S): Lithosphere, v. 9, p. 453–462, https://doi.org/10.1130/L546.1.

Barazangi, M., and Isacks, B.L., 1976, Spatial distribution of earthquakes and subduction of the Nazca plate beneath South America: Geology, v. 4, no. 11, p. 686–692, https://doi.org/10.1130/0091-7613(1976)4<686:SDOEAS>2.0.CO;2.

Barber, D.E., Stockli, D.F., and Galster, F., 2019, The proto–Zagros foreland basin in Lorestan, western Iran—Insights from multi-mineral detrital geo-thermochronometric and trace-elemental provenance analysis: Geochemistry Geophysics Geosystems, v. 20, p. 2657–2680, https://doi.org/10.1029/2019GC008185.

Barredo, S.P., 2012, Geodynamic and tectonostratigraphic study of a continental rift: The Triassic Cuyana Basin, Argentina, *in* Sharkov, E., ed., Tectonics—Recent Advances: InTechOpen, p. 32, https://doi.org/10.5772/49958.

Belousova, E., Griffin, W.L., O'Reilly, S.Y., and Fisher, N.L., 2002, Igneous zircon: Trace element composition as an indicator of source rock type: Contributions to Mineralogy and Petrology, v. 143, no. 5, p. 602–622, https://doi.org/10.1007/s00410-002-0364-7.

Belousova, E.A., Kostitsyn, Y.A., Griffin, W.L., Begg, G.C., O'Reilly, S.Y., and Pearson, N.J., 2010, The growth of the continental crust: Constraints from zircon Hf-isotope data: Lithos, v. 119, no. 3–4, p. 457–466, https://doi.org/10.1016/j.lithos.2010.07.024.

Bianchi, M., Heit, B., Jakovlev, A., Yuan, X., Kay, S.M., Sandvol, E., Alonso, R.N., Coira, B., Brown, L., Kind, R., and Comte, D., 2013, Teleseismic tomography of the southern Puna plateau in Argentina and adjacent regions: Tectonophysics, v. 586, p. 65–83, https://doi.org/10.1016/j.tecto.2012.11.016.

Bouvier, A., Vervoort, J.D., and Patchett, P.J., 2008, The Lu-Hf and Sm-Nd isotopic composition of CHUR: Constraints from unequilibrated chondrites and implications for the bulk composition of terrestrial planets: Earth and Planetary Science Letters, v. 273, p. 48–57, https://doi.org/10.1016/j.epsl.2008.06.010.

Buelow, E.K., Suriano, J., Mahoney, J.B., Kimbrough, D.L., Mescua, J.F., Giambiagi, L.B., and Hoke, G.D., 2018, Sedimentologic and stratigraphic evolution of the Cacheuta basin: Constraints on the development of the Miocene retroarc foreland basin, south-central Andes: Lithosphere, v. 10, no. 3, p. 366–391, https://doi.org/10.1130/L709.1.

Butler, K.L., Horton, B.K., Echaurren, A., Folguera, A., and Fuentes, F., 2019, Cretaceous–Cenozoic growth of the Patagonian broken foreland basin, Argentina: Chronostratigraphic framework and provenance variations during transitions in Andean subduction dynamics: Journal of South American Earth Sciences, v. 97, p. 102242, https://doi.org/10.1016/j.jsames.2019.102242.

Capaldi, T.N., Horton, B.K., McKenzie, N.R., Stockli, D.F., and Odlum, M.L., 2017, Sediment provenance in contractional orogens: The detrital zircon record from modern rivers in the Andean fold-thrust belt and foreland basin of western Argentina: Earth and Planetary Science Letters, v. 479, p. 83–97, https://doi.org/10.1016/j.epsl.2017.09.001.

Capaldi, T.N., Horton, B.K., McKenzie, N.R., Mackaman-Lofland, C., Stockli, D.F., Ortiz, G., and Alvarado, P., 2020, Neogene retroarc foreland basin evolution, sediment provenance, and magmatism in response to flat slab subduction, western Argentina: Tectonics, v. 39, no. 7, https://doi.org/10.1029/2019TC005958.

Carrapa, B., and DeCelles, P.G., 2015, Regional exhumation and kinematic history of the Central Andes in response to cyclical orogenic processes, *in* DeCelles, P.G., Ducea, M.N., Carrapa, B., and Kapp, P.A., eds., Geodynamics of a Cordilleran Orogenic System: The Central Andes of Argentina and Northern Chile: Geological Society of America Memoir 212, p. 201–213, https://doi.org/10.1130/2015.1212(11).

Casquet, C., Baldo, E., Pankhurst, R.J., Rapela, C.W., Galindo, C., Fanning, C.M., and Saaverdra, J., 2001, Involvement of the Argentine Precordillera terrane in the Famatinian mobile belt: U-Pb SHRIMP and metamorphic evidence from the Sierra de Pie de Palo: Geology, v. 29, p. 703–706, https://doi.org/10.1130/0091-7613(2001)029<0703:IOTAPT>2.0.CO;2.

Cawood, P.A., 2005, Terra Australis orogen: Rodinia breakup and development of the Pacific and Iapetus margins of Gondwana during the Neoproterozoic and Paleozoic: Earth-Science Reviews, v. 69, p. 249–279, https://doi.org/10.1016/j.earscirev.2004.09.001.

Cawood, P.A., Hawkesworth, C.J., and Dhuime, B., 2012, Detrital zircon record and tectonic setting: Geology, v. 40, p. 875–878, https://doi.org/10.1130/G32945.1.

Chapman, J.B., and Ducea, M.N., 2019, The role of arc migration in Cordilleran orogenic cyclicity: Geology, v. 47, p. 627–631, https://doi.org/10.1130/G46117.1.

Chapman, J.B., Ducea, M.N., Kapp, P., Gehrels, G.E., and DeCelles, P.G., 2017, Spatial and temporal radiogenic isotopic trends of magmatism in Cordillera orogens: Gondwana Research, v. 48, p. 189–204, https://doi.org/10.1016/j.gr.2017.04.019.

Charrier, R., Baeza, O., Elgueta, S., Flynn, J.J., Gans, P., Kay, S.M., Muñoz, N., Wyss, A.R., and Zurita, E., 2002, Evidence for Cenozoic extensional basin development and tectonic inversion south of the flat-slab segment, southern Central Andes, Chile (33–36°SL): Journal of South American Earth Sciences, v. 15, no. 1, p. 117–139, https://doi.org/10.1016/S0895-9811(02)00009-3.

Charrier, R., Ramos, V.A., Tapia, F., and Sagripanti, L., 2015, Tecto-no-stratigraphic evolution of the Andean orogen between 31 and 37°S (Chile and western Argentina), *in* Sepúlveda, S.A., et al., eds., Geodynamic Processes in the Andes of Central Chile and Argentina: Geological Society [London] Special Publication 399, p. 13–61, https://doi.org/10.1144/SP399.20.

Chen, Y.W., Wu, J., and Suppe, J., 2019, Southward propagation of Nazca subduction along the Andes: Nature, v. 565, no. 7740, p. 441, https://doi.org/10.1038/s41586-018-0860-1.

Coira, B.L., Davidson, J.D., Mpodozis, C., and Ramos, V.A., 1982, Tectonic and magmatic evolution of the Andes of northern Argentina and Chile: Earth-Science Reviews, v. 18, p. 303–332, https://doi.org/10.1016/0012-8252(82)90042-3.

Coloma, F., Valin, X., Oliveros, V., Vásquez, P., Creixell, C., Salazar, E., and Ducea, M.N., 2017, Geoquímica de rocas ígneas Permo-Triásicas del norte de Chile (28°–30°15′S): Implicancias en la dinámica del margen pre-Andino: Andean Geology, v. 44, p. 147–178, https://doi.org/10.5027/andgeoV44n2-a03.

Condie, K.C., Bickford, M.E., Aster, R.C., Belousova, E., and Scholl, D.W., 2011, Episodic zircon ages, Hf isotopic composition, and the preservation rate of continental crust: Geological Society of America Bulletin, v. 123, p. 951–957, https://doi.org/10.1130/B30344.1.

Coney, P.J., and Reynolds, S.J., 1977, Cordilleran Benioff zones: Nature, v. 270, no. 5636, p. 403–406, https://doi.org/10.1038/270403a0.

Cristallini, E.O., and Ramos, V.A., 2000, Thick-skinned and thin-skinned thrusting in the La Ramada fold and thrust belt: Crustal evolution of the High Andes of San Juan, Argentina (32°SL): Tectonophysics, v. 317, p. 205–235, https://doi.org/10.1016/S0040-1951(99)00276-0.

Cristofolini, E.A., Otamendi, J.E., Ducea, M.N., Pearson, D.M., Tibaldi, A.M., and Baliani, I., 2012, Detrital zircon U-Pb ages of metasedimentary rocks from Sierra de Valle Fértil: Entrapment of middle and late Cambrian marine successions in the deep roots of the Early Ordovician Famatinian arc: Journal of South American Earth Sciences, v. 37, p. 77–94, https://doi.org/10.1016/j.jsames.2012.02.001.

Currie, B.S., Colombi, C.E., Tabor, N.J., Shipman, T.C., and Montañez, I.P., 2009, Stratigraphy and architecture of the Upper Triassic Ischigualasto Formation, Ischigualasto Provincial Park, San Juan, Argentina: Journal of South American Earth Sciences, v. 27, p. 74–87, https://doi.org/10.1016/j.jsames.2008.10.004.

Currie, C.A., Ducea, M.N., DeCelles, P.G., and Beaumont, C., 2015, Geodynamic models of Cordilleran orogens: Gravitational instability of magmatic arc roots, *in* DeCelles, P.G., Ducea, M.N., Carrapa, B., and Kapp, P.A., eds., Geodynamics of a Cordilleran Orogenic System: The Central Andes of Argentina and Northern Chile: Geological Society of America Memoir 212, p. 1–22, https://doi.org/10.1130/2015.1212(01).

Dahlquist, J.A., Pankhurst, R.J., Gaschnig, R.M., Rapela, C.W., Casquet, C., Alasino, P.H., Galindo, C., and Baldo, E.G., 2013, Hf and Nd isotopes in Early Ordovician to early Carboniferous granites as monitors of crustal growth in the proto-Andean margin of Gondwana: Gondwana Research, v. 23, p. 1617–1630, https://doi.org/10.1016/j.gr.2012.08.013.

Dahlquist, J.A., Verdecchia, S.O., Baldo, E.G., Basei, M.A.S., Alasino, P.H., Urán, G.A., Rapela, C.W., da Costa Campos, M., and Zandomeni, P.S., 2016, Edad U-Pb y análisis isotópico de Hf en circones del plutón Guasayán del Cámbrico temprano, Sierras Pampeanas, Argentina: Implicancias para el límite noroccidental del arco pampeano: Andean Geology, v. 43, p. 137–150, https://doi.org/10.5027/andgeoV43n1-a08.

Dahlquist, J.A., Alasino, P.H., Basei, M.A.S., Morales Cámera, M.M., Macchioli Grande, M., and da Costa Campos Neto, M., 2018, Petrological, geochemical, isotopic, and geochronological constraints for the Late Devonian–early Carboniferous magmatism in SW Gondwana (27–32°LS): An example of geodynamic switching: International Journal of Earth Sciences, v. 107, p. 2575–2603, https://doi.org/10.1007/s00531-018-1615-9.

DeCelles, P.G., Ducea, M.N., Kapp, P., and Zandt, G., 2009, Cyclicity in Cordilleran orogenic systems: Nature Geoscience, v. 2, no. 4, p. 251–257, https://doi.org/10.1038/ngeo469.

DeCelles, P.G., Zandt, G., Beck, S.L., Currie, C.A., Ducea, M.N., Kapp, P., Gehrels, G.E., Carrapa, B., and Quade, J., 2015, Cyclical orogenic processes in the Cenozoic Central Andes, *in* DeCelles, P.G., Ducea, M.N., Carrapa, B., and Kapp, P.A., eds., Geodynamics of a Cordilleran Orogenic System: The Central Andes of Argentina and Northern Chile: Geological Society of America Memoir 212, p. 459–490, https://doi.org/10.1130/2015.1212(22).

del Rey, A., Deckart, K., Arriagada, C., and Martínez, F., 2016, Resolving the paradigm of the late Paleozoic–Triassic Chilean magmatism: Isotopic approach: Gondwana Research, v. 37, p. 172–181, https://doi.org/10.1016/j.gr.2016.06.008.

de Silva, S.L., and Kay, S.M., 2018, Turning up the heat: High-flux magmatism in the Central Andes: Elements, v. 14, p. 245–250, https://doi.org/10.2138/gselements.14.4.245.

de Silva, S.L., Riggs, N.R., and Barth, A.P., 2015, Quickening the pulse: Fractal tempos in continental arc magmatism: Elements, v. 11, p. 113–118, https://doi.org/10.2113/gselements.11.2.113.

Dhuime, B., Hawkesworth, C.J., Delavault, H., and Cawood, P.A., 2017, Continental growth seen through the sedimentary record: Sedimentary Geology, v. 357, p. 16–32, https://doi.org/10.1016/j.sedgeo.2017.06.001.

Dickinson, W.R., 1973, Widths of modern arc-trench gaps proportional to past duration of igneous activity in associated magmatic arcs: Journal of Geophysical Research, v. 78, p. 3376–3389, https://doi.org/10.1029/JB078i017p03376.

Dickinson, W.R., 1975, Potash-depth (K-*h*) relations in continental margin and intra-oceanic magmatic arcs: Geology, v. 3, p. 53–56, https://doi.org/10.1130/0091-7613(1975)3<53:PKRICM>2.0.CO;2.

Ducea, M.N., Otamendi, J.E., Bergantz, G., Stair, K.M., Valencia, V.A., and Gehrels, G., 2010, Timing constraints on building

an intermediate plutonic arc crustal section: U-Pb zircon geochronology of the Sierra Valle Fertil–La Huerta, Famatinian arc, Argentina: Tectonics, v. 29, TC4002, https://doi.org/10.1029/2009TC002615.

Ducea, M.N., Paterson, S.R., and DeCelles, P.G., 2015, High-volume magmatic events in subduction systems: Elements, v. 11, no. 2, p. 99–104, https://doi.org/10.2113/gselements.11.2.99.

Elhlou, S., Belousova, E., Griffin, W.L., Pearson, N.J., and O'Reilly, S.Y., 2006, Trace element and isotopic composition of GJ-red zircon standard by laser ablation: Geochimica et Cosmochimica Acta, v. 70, p. A158, https://doi.org/10.1016/j.gca.2006.06.1383.

Faccenna, C., Oncken, O., Holt, A.F., and Becker, T.W., 2017, Initiation of the Andean orogeny by lower mantle subduction: Earth and Planetary Science Letters, v. 463, p. 189–201, https://doi.org/10.1016/j.epsl.2017.01.041.

Farías, M., Charrier, R., Carretier, S., Martinod, J., Fock, A., Campbell, D., Cáceres, J., and Comte, D., 2008, Late Miocene high and rapid surface uplift and its erosional response in the Andes of central Chile (33–35°S): Tectonics, v. 27, no. 1, TC1005, https://doi.org/10.1029/2006TC002046.

Folguera, A., and Ramos, V.A., 2011, Repeated eastward shifts of arc magmatism in the Southern Andes: A revision to the long-term pattern of Andean uplift and magmatism: Journal of South American Earth Sciences, v. 32, p. 531–546, https://doi.org/10.1016/j.jsames.2011.04.003.

Folguera, A., Zapata, T., and Ramos, V.A., 2006, Late Cenozoic extension and the evolution of the Neuquén Andes, *in* Kay, S.M., and Ramos, V.A., eds., Evolution of an Andean Margin: A Tectonic and Magmatic View from the Andes to the Neuquén Basin (35°–39°S Lat): Geological Society of America Special Paper 407, p. 267–285, https://doi.org/10.1130/2006.2407(12).

Fosdick, J.C., Carrapa, B., and Ortíz, G., 2015, Faulting and erosion in the Argentine Precordillera during changes in subduction regime: Reconciling bedrock cooling and detrital records: Earth and Planetary Science Letters, v. 432, p. 73–83, https://doi.org/10.1016/j.epsl.2015.09.041.

Fosdick, J.C., Reat, E.J., Carrapa, B., Ortiz, G., and Alvarado, P.M., 2017, Retroarc basin reorganization and aridification during Paleogene uplift of the southern central Andes: Tectonics, v. 36, no. 3, p. 493–514, https://doi.org/10.1002/2016TC004400.

Franzese, J.R., and Spalletti, L.A., 2001, Late Triassic–Early Jurassic continental extension in south western Gondwana: Tectonic segmentation and pre-break-up rifting: Journal of South American Earth Sciences, v. 14, p. 257–270, https://doi.org/10.1016/S0895-9811(01)00029-3.

Gehrels, G., 2014, Detrital zircon U-Pb geochronology applied to tectonics: Annual Review of Earth and Planetary Sciences, v. 42, p. 127–149, https://doi.org/10.1146/annurev-earth-050212-124012.

Giambiagi, L., Mescua, J., Heredia, N., Farias, P., Garcia Sansegundo, J., Fernandez, C., Stier, S., Perez, D., Bechis, F., Moreiras, S.M., and Lossada, A., 2014, Reactivation of Paleozoic structures during Cenozoic deformation in the Cordón del Plata and Southern Precordillera ranges (Mendoza, Argentina): Journal of Iberian Geology, v. 40, p. 309–320, https://doi.org/10.5209/rev_JIGE.2014.v40.n2.45302.

Giambiagi, L., Tassara, A., Mescua, J., Tunik, M., Alvarez, P.P., Godoy, E., Hoke, G., Pinto, L., Spagnotto, S., Porras, H., Tapia, F., Jara, P., Bechis, F., García V., Suriano, J., Maris-Moreiras, S., and Pagano, S., 2015, Evolution of shallow and deep structures along the Maipo-Tunuyán transect (33°40′S): From the Pacific coast to the Andean foreland, *in* Sepúlveda, S.A., et al., eds., Geodynamic Processes in the Andes of Central Chile and Argentina: Geological Society of London Special Publication 399, p. 63–82, https://doi.org/10.1144/SP399.14.

Gilbert, H., Beck, S., and Zandt, G., 2006, Lithospheric and upper mantle structure of central Chile and Argentina: Geophysical Journal International, v. 165, p. 383–398, https://doi.org/10.1111/j.1365-246X.2006.02867.x.

Global Volcanism Program, 2013, Volcanoes of the World, V. 4.9.0 (04 Jun 2020; Venzke, E., ed.): Washington, D.C., Smithsonian Institution (downloaded 15 June 2020), https://doi.org/10.5479/si.GVP.VOTW4-2013.

González, J., Oliveros, V., Creixell, C., Velásquez, R., Vásquez, P., and Lucassen, F., 2018, The Triassic magmatism and its relation with the pre-Andean tectonic evolution: Geochemical and petrographic constraints from the High Andes of north central Chile (29°30′– 30°S): Journal of South American Earth Sciences, v. 87, p. 95–112, https://doi.org/10.1016/j.jsames.2017.12.009.

Haschke, M., Siebel, W., Günther, A., and Scheuber, E., 2002, Repeated crustal thickening and recycling during the Andean orogeny in north Chile (21°–26°S): Journal of Geophysical Research, v. 107, p. ECV 6-1–ECV 6-18, https://doi.org/10.1029/2001JB000328.

Haschke, M., Günther, A., Melnick, D., Echtler, H., Reutter, K.J., Scheuber, E., and Oncken, O., 2006, Central and southern Andean tectonic evolution inferred from arc magmatism, *in* Oncken, O., et al., eds., The Andes: Frontiers in Earth Sciences: Berlin, Springer, p. 337–353, https://doi.org/10.1007/978-3-540-48684-8_16.

Hawkesworth, C.J., and Kemp, A.I.S., 2006, Using hafnium and oxygen isotopes in zircons to unravel the record of crustal evolution: Chemical Geology, v. 226, p. 144–162, https://doi.org/10.1016/j.chemgeo.2005.09.018.

Hayes, G.P., Moore, G.L., Portner, D.E., Hearne, M., Flamme, H., Furtney, M., and Smoczyk, G.M., 2018, Slab2, a comprehensive subduction zone geometry model: Science, v. 362, p. 58–61, https://doi.org/10.1126/science.aat4723.

Hervé, F., Calderón, M., Fanning, C.M., Pankhurst, R.J., and Godoy, E., 2013, Provenance variations in the Late Paleozoic accretionary complex of central Chile as indicated by detrital zircons: Gondwana Research, v. 23, p. 1122–1135, https://doi.org/10.1016/j.gr.2012.06.016.

Hervé, F., Fanning, C.M., Calderon, M., and Mpodozis, C., 2014, Early Permian to Late Triassic batholiths of the Chilean Frontal Cordillera (28–31°S): SHRIMP U-Pb zircon ages and Lu-Hf and O isotope systems: Lithos, v. 187, p. 436–446, https://doi.org/10.1016/j.lithos.2013.10.018.

Heuret, A., and Lallemand, S., 2005, Plate motions, slab dynamics and back-arc deformation: Physics of the Earth and Planetary Interiors, v. 149, p. 31–51, https://doi.org/10.1016/j.pepi.2004.08.022.

Hildreth, W., and Moorbath, S., 1988, Crustal contributions to arc magmatism in the Andes of central Chile: Contributions to Mineralogy and Petrology, v. 98, p. 455–489, https://doi.org/10.1007/BF00372365.

Horton, B.K., 2018a, Tectonic regimes of the central and southern Andes: Responses to variations in plate coupling during subduction: Tectonics, v. 37, p. 402–429, https://doi.org/10.1002/2017TC004624.

Horton, B.K., 2018b, Sedimentary record of Andean mountain building: Earth-Science Reviews, v. 178, p. 279–309, https://doi.org/10.1016/j.earscirev.2017.11.025.

Horton, B.K., and Fuentes, F., 2016, Sedimentary record of plate coupling and decoupling during growth of the Andes: Geology, v. 44, p. 647–650, https://doi.org/10.1130/G37918.1.

Horton, B.K., Anderson, V.J., Caballero, V., Saylor, J.E., Parra, M., and Mora, A., 2015, Application of detrital zircon U-Pb geochronology to surface and subsurface correlations of provenance, paleodrainage, and tectonics of the Middle Magdalena Valley Basin of Colombia: Geosphere, v. 11, p. 1790–1811, https://doi.org/10.1130/GES01251.1.

Horton, B.K., Fuentes, F., Boll, A., Starck, D., Ramirez, S.G., and Stockli, D.F., 2016, Andean stratigraphic record of the transition from backarc extension to orogenic shortening: A case study from the northern Neuquén Basin, Argentina: Journal of South American Earth Sciences, v. 71, p. 17–40, https://doi.org/10.1016/j.jsames.2016.06.003.

Husson, L., Conrad, C.P., and Faccenna, C., 2012, Plate motions, Andean orogeny, and volcanism above the South Atlantic convection cell: Earth and Planetary Science Letters, v. 317–318, p. 126–135, https://doi.org/10.1016/j.epsl.2011.11.040.

Isacks, B.L., 1988, Uplift of the central Andean Plateau and bending of the Bolivian orocline: Journal of Geophysical Research, v. 93, p. 3211–3231, https://doi.org/10.1029/JB093iB04p03211.

Jackson, S.E., Pearson, N.J., Griffin, W.L., and Belousova, E.A., 2004, The application of laser ablation–inductively coupled plasma–mass spectrometry to in situ U-Pb zircon geochronology: Chemical Geology, v. 211, p. 47–69, https://doi.org/10.1016/j.chemgeo.2004.06.017.

Jacob, K.H., Nakamura, K., and Davies, J.N., 1977, Trench-volcano gap along the Alaska-Aleutian arc: Island arcs, *in* Talwani, M., and Pitman, W.C., Jr., eds., Deep Sea Trenches and Back-Arc Basins: New York, Wiley, p. 243–258, https://doi.org/10.1029/ME001p0243.

Jarrard, R.D., 1986, Relations among subduction parameters: Reviews of Geophysics, v. 24, p. 217–284, https://doi.org/10.1029/RG024i002p00217.

Jones, R.E., Kirstein, L.A., Kasemann, S.A., Dhuime, B., Elliott, T., Litvak, V.D., Alonso, R.N., and Hinton, R., 2015, Geodynamic controls on the contamination of Cenozoic arc magmas in the southern Central Andes: Insights from the O and Hf isotopic composition of zircon: Geochimica et Cosmochimica Acta, v. 164, p. 386–402, https://doi.org/10.1016/j.gca.2015.05.007.

Jones, R.E., Kirstein, L.A., Kasemann, S.A., Litvak, V.D., Poma, S., Alonso, R.N., and Hinton, R., 2016, The role of changing geodynamics in the progressive contamination of Late Cretaceous to late Miocene arc magmas in the southern Central Andes: Lithos, v. 262, p. 169–191, https://doi.org/10.1016/j.lithos.2016.07.002.

Jordan, T.E., Isacks, B.L., Allmendinger, R.W., Brewer, J.A., Ramos, V.A., and Ando, C.J., 1983, Andean tectonics related to geometry of subducted Nazca plate: Geological Society of America Bulletin, v. 94, p. 341–361, https://doi.org/10.1130/0016-7606(1983)94<341:ATRTGO>2.0.CO;2.

Jordan, T.E., Allmendinger, R.W., Damanti, J.F., and Drake, R.E., 1993, Chronology of motion in a complete thrust belt: The

Precordillera 30–31°S, Andes Mountains: The Journal of Geology, v. 101, p. 135–156, https://doi.org/10.1086/648213.

Kay, S.M., and Abbruzzi, J.M., 1996, Magmatic evidence for Neogene lithospheric evolution of the central Andean "flat-slab" between 30°S and 32°S: Tectonophysics, v. 259, p. 15–28, https://doi.org/10.1016/0040-1951(96)00032-7.

Kay, S.M., and Mpodozis, C., 2002, Magmatism as a probe to the Neogene shallowing of the Nazca plate beneath the modern Chilean flat-slab: Journal of South American Earth Sciences, v. 15, p. 39–57, https://doi.org/10.1016/S0895-9811(02)00005-6.

Kay, S.M., Maksaev, V., Moscoso, R., Mpodozis, C., and Nasi, C., 1987, Probing the evolving Andean lithosphere: Mid-late Tertiary magmatism in Chile (29°–30°30′S) over the modern zone of subhorizontal subduction: Journal of Geophysical Research–Solid Earth, v. 92, no. B7, p. 6173–6189, https://doi.org/10.1029/JB092iB07p06173.

Kay, S.M., Ramos, V.A., Mpodozis, C., and Sruoga, P., 1989, Late Paleozoic to Jurassic silicic magmatism at the Gondwana margin: Analogy to the Middle Proterozoic in North America?: Geology, v. 17, p. 324–328, https://doi.org/10.1130/0091-7613(1989)017<0324:LPTJSM>2.3.CO;2.

Kay, S.M., Mpodozis, C., Ramos, V.A., and Munizaga, F., 1991, Magma source variations for mid-late Tertiary magmatic rocks associated with a shallowing subduction zone and a thickening crust in the central Andes (28 to 33°S), *in* Harmon, R.S., and Rapela. C.W., eds., Andean Magmatism and its Tectonic Setting: Geological Society of America Special Paper 265, p. 113–137, https://doi.org/10.1130/SPE265-p113.

Kay, S.M., Godoy, E., and Kurtz, A., 2005, Episodic arc migration, crustal thickening, subduction erosion, and magmatism in the south-central Andes: Geological Society of America Bulletin, v. 117, no. 1–2, p. 67–88, https://doi.org/10.1130/B25431.1.

Keith, S.B., 1978, Paleosubduction geometries inferred from Cretaceous and Tertiary magmatic patterns in southwestern North America: Geology, v. 6, p. 516–521, https://doi.org/10.1130/0091-7613(1978)6<516:PGIFCA>2.0.CO;2.

Keith, S.B., 1982, Paleoconvergence rates determined from K_2O/SiO_2 ratios in magmatic rocks and their application to Cretaceous and Tertiary tectonic patterns in southwestern North America: Geological Society of America Bulletin, v. 93, p. 524–532, https://doi.org/10.1130/0016-7606(1982)93<524:PRDFSR>2.0.CO;2.

Kemp, A.I.S., Hawkesworth, C.J., Paterson, B.A., Kinny, P.D., and Kemp, T., 2006, Episodic growth of the Gondwana supercontinent from hafnium and oxygen isotopes in zircon: Nature, v. 439, p. 580–583, https://doi.org/10.1038/nature04505.

Kemp, A.I.S., Hawkesworth, C.J., Collins, W.J., Gray, C.M., and Blevin, P.L., 2009, Isotopic evidence for rapid continental growth in an extensional accretionary orogen: The Tasmanides, eastern Australia: Earth and Planetary Science Letters, v. 284, p. 455–466, https://doi.org/10.1016/j.epsl.2009.05.011.

Kent, D.V., Malnis, P.S., Colombi, C.E., Alcober, O.A., and Martínez, R.N., 2014, Age constraints on the dispersal of dinosaurs in the Late Triassic from magnetochronology of the Los Colorados Formation (Argentina): Proceedings of the National Academy of Sciences of the United States of America, v. 111, p. 7958–7963, https://doi.org/10.1073/pnas.1402369111.

Kirkland, C.L., Smithies, R.H., Taylor, R.J.M., Evans, N., and McDonald, B., 2015, Zircon Th/U ratios in magmatic environs: Lithos, v. 212, p. 397–414, https://doi.org/10.1016/j.lithos.2014.11.021.

Kirsch, M., Paterson, S.R., Wobbe, F., Ardila, A.M.M., Clausen, B.L., and Alasino, P.H., 2016, Temporal histories of Cordilleran continental arcs: Testing models for magmatic episodicity: The American Mineralogist, v. 101, no. 10, p. 2133–2154, https://doi.org/10.2138/am-2016-5718.

Kleiman, L.E., and Japas, M.S., 2009, The Choiyoi volcanic province at 34°S–36°S (San Rafael, Mendoza, Argentina): Implications for the late Paleozoic evolution of the southwestern margin of Gondwana: Tectonophysics, v. 473, no. 3–4, p. 283–299, https://doi.org/10.1016/j.tecto.2009.02.046.

Levina, M., Horton, B.K., Fuentes, F., and Stockli, D.F., 2014, Cenozoic sedimentation and exhumation of the foreland basin system preserved in the Precordillera thrust belt (31–32°S), southern central Andes, Argentina: Tectonics, v. 33, no. 9. p. 1659–1680, https://doi.org/10.1002/2013TC003424.

Litvak, V.D., and Poma, S., 2010, Geochemistry of mafic Paleocene volcanic rocks in the Valle del Cura region: Implications for the petrogenesis of primary mantle–derived melts over the Pampean flat-slab: Journal of South American Earth Sciences, v. 29, p. 705–716, https://doi.org/10.1016/j.jsames.2010.01.001.

Litvak, V.D., Poma, S., and Kay, S.M., 2007, Paleogene and Neogene magmatism in the Valle del Cura region: New perspective on the evolution of the Pampean flat slab, San Juan province, Argentina: Journal of South American Earth Sciences, v. 24, no. 2–4, p. 117–137, https://doi.org/10.1016/j.jsames.2007.04.002.

Litvak, V.D., Poma, S., Jones, R.E., Fernández Paz, L., Iannelli, S.B., Spagnuolo, M., Kirstein, L.A., Folguera, A., and Ramos, V.A., 2018, The late Paleogene to Neogene volcanic arc in the southern Central Andes (28°–37°S), *in* Folguera, A., et al., eds., The Evolution of the Chilean-Argentinean Andes: Cham, Switzerland, Springer, p. 503–536, https://doi.org/10.1007/978-3-319-67774-3_20.

Llambías, E.J., and Sato, A.M., 1995, El batolito de Colangüil: Transición entre orogénesis y anorogénesis: Revista de la Asociación Geológica Argentina, v. 50, p. 111–131.

Llambías, E.J., Quenardelle, S., and Montenegro, T., 2003, The Choiyoi Group from central Argentina: A subalkaline transitional to alkaline association in the craton adjacent to the active margin of the Gondwana continent: Journal of South American Earth Sciences, v. 16, p. 243–257, https://doi.org/10.1016/S0895-9811(03)00070-1.

Lossada, A.C., Giambiagi, L., Hoke, G.D., Fitzgerald, P.G., Creixell, C., Murillo, I., Mardonez, D., Velásquez, R., and Suriano, J., 2017, Thermochronologic evidence for late Eocene Andean mountain building at 30°S: Tectonics, v. 36, p. 2693–2713, https://doi.org/10.1002/2017TC004674.

Mackaman-Lofland, C., Horton, B.K., Fuentes, F., Constenius, K.N., and Stockli, D.F., 2019, Mesozoic to Cenozoic retroarc basin evolution during changes in tectonic regime, southern Central Andes (31–33°S): Insights from zircon U-Pb geochronology: Journal of South American Earth Sciences, v. 89, p. 299–318, https://doi.org/10.1016/j.jsames.2018.10.004.

Mackaman-Lofland, C., Horton, B.K., Fuentes, F., Constenius, K.N., Ketcham, R.A., Capaldi, T.N., Stockli, D.F., Ammirati, J.B., Alvarado, P., and Orozco, P., 2020, Andean mountain building and foreland basin evolution during thin- and thick-skinned Neogene deformation (32–33°S): Tectonics, v. 39, no. 3, https://doi.org/10.1029/2019TC005838.

Maloney, K.T., Geoffrey, L.C., Klepeis, K.A., and Quevedo, L., 2013, The Late Jurassic to present evolution of the Andean margin: Drivers and the geologic record: Tectonics, v. 32, p. 1049–1065, https://doi.org/10.1002/tect.20067.

Martin, E.L., Collins, W.J., and Spencer, C.J., 2019, Laurentian origin of the Cuyania suspect terrane, western Argentina, confirmed by Hf isotopes in zircon: Geological Society of America Bulletin, v. 132, p. 273–290, https://doi.org/10.1130/B35150.1.

Martinod, J., Husson, L., Roperch, P., Guillaume, B., and Espurt, N., 2010, Horizontal subduction zones, convergence velocity and the building of the Andes: Earth and Planetary Science Letters, v. 299, p. 299–309, https://doi.org/10.1016/j.epsl.2010.09.010.

McKay, M.P., Jackson, W.T., and Hessler, A.M., 2018, Tectonic stress regime recorded by zircon Th/U: Gondwana Research, v. 57, p. 1–9, https://doi.org/10.1016/j.gr.2018.01.004.

McKenzie, N.R., Smye, A.J., Hegde, V.S., and Stockli, D.F., 2018, Continental growth histories revealed by detrital zircon trace elements: A case study from India: Geology, v. 46, p. 275–278, https://doi.org/10.1130/G39973.1.

Moreno, J.A., Dahlquist, J.A., Morales Cámera, M.M., Alasino, P.H., Larrovere, M.A., Basei, M.A.S., Galindo, C., Zandomeni, P.S., and Rocher, S., 2020, Geochronology and geochemistry of the Tabaquito batholith (Frontal Cordillera, Argentina): Geodynamic implications and temporal correlations in the SW Gondwana margin: Journal of the Geological Society [London], v. 177, p. 455–474, https://doi.org/10.1144/jgs2019-062.

Mosolf, J.G., Gans, P.B., Wyss, A.R., Cottle, J.M., and Flynn, J.J., 2019, Late Cretaceous to Miocene volcanism, sedimentation, and upper-crustal faulting and folding in the Principal Cordillera, central Chile: Field and geochronological evidence for protracted arc volcanism and transpressive deformation: Geological Society of America Bulletin, v. 131, p. 252–273, https://doi.org/10.1130/B31998.1.

Mpodozis, C., and Kay, S.M., 1992, Late Paleozoic to Triassic evolution of the Gondwana margin: Evidence from Chilean Frontal Cordilleran batholiths (28 to 31°S): Geological Society of America Bulletin, v. 104, p. 999–1014, https://doi.org/10.1130/0016-7606(1992)104<0999:LPTTEO>2.3.CO;2.

Nelson, D.A., and Cottle, J.M., 2019, Tracking voluminous Permian volcanism of the Choiyoi Province into central Antarctica: Lithosphere, v. 11, p. 386–398, https://doi.org/10.1130/L1015.1.

Odlum, M.L., Stockli, D.F., Capaldi, T.N., Thomson, K.D., Clark, J., Puigdefàbregas, C., and Fildani, A., 2019, Tectonic and sediment provenance evolution of the south eastern Pyrenean foreland basins during rift margin inversion and orogenic uplift: Tectonophysics, v. 765, p. 226–248, https://doi.org/10.1016/j.tecto.2019.05.008.

Oliveros, V., Labbé, M., Rossel, P., Charrier, R., and Encinas, A., 2012, Late Jurassic paleogeographic evolution of the Andean back-arc basin: New constraints from the Lagunillas Formation, northern Chile (27°30′–28°30′S): Journal of South American Earth Sciences, v. 37, p. 25–40, https://doi.org/10.1016/j.jsames.2011.12.005.

Oliveros, V., González, J., Vargas, M.E., Vásquez, P., Rossel, P., Creixell, C., Sepúlveda, F., and Bastias, F., 2018, The early stages of the magmatic arc in the southern Central Andes,

in Folguera, A., et al., eds., The Evolution of the Chilean-Argentinean Andes: Cham, Switzerland, Springer, p. 165–190, https://doi.org/10.1007/978-3-319-67774-3_7.

Otamendi, J.E., Ducea, M.N., Cristofolini, E.A., Tibaldi, A.M., Camilletti, G.C., and Bergantz, G.W., 2017, U-Pb ages and Hf isotope compositions of zircons in plutonic rocks from the central Famatinian arc, Argentina: Journal of South American Earth Sciences, v. 76, p. 412–426, https://doi.org/10.1016/j.jsames.2017.04.005.

Pankhurst, R.J., Rapela, C.W., Fanning, C.M., and Márquez, M., 2006, Gondwanide continental collision and the origin of Patagonia: Earth-Science Reviews, v. 76, p. 235–257, https://doi.org/10.1016/j.earscirev.2006.02.001.

Parada, M.A., Rivano, S., Sepulveda, P., Herve, M., Herve, F., Puig, A., Munizaga, F., Brook, M., Pankhurst, R., and Snelling, N., 1988, Mesozoic and Cenozoic plutonic development in the Andes of central Chile (30°30′–32°30′S): Journal of South American Earth Sciences, v. 1, p. 249–260, https://doi.org/10.1016/0895-9811(88)90003-X.

Parada, M.A., Nyström, J.O., and Levi, B., 1999, Multiple sources for the Coastal Batholith of central Chile (31–34°S): Geochemical and Sr-Nd isotopic evidence and tectonic implications: Lithos, v. 46, no. 3, p. 505–521, https://doi.org/10.1016/S0024-4937(98)00080-2.

Parada, M.A., Féraud, G., Fuentes, F., Aguirre, L., Morata, D., and Larrondo, P., 2005, Ages and cooling history of the Early Cretaceous Caleu pluton: Testimony of a switch from a rifted to a compressional continental margin in central Chile: Journal of the Geological Society [London], v. 162, p. 273–287, https://doi.org/10.1144/0016-764903-173.

Paterson, S.R., and Ducea, M.N., 2015, Arc magmatic tempos: Gathering the evidence: Elements, v. 11, p. 91–98, https://doi.org/10.2113/gselements.11.2.91.

Peacock, S.M., Rushmer, T., and Thompson, A.B., 1994, Partial melting of subducting oceanic crust: Earth and Planetary Science Letters, v. 121, p. 227–244, https://doi.org/10.1016/0012-821X(94)90042-6.

Pepper, M.B., Gehrels, G., Pullen, A., Ibanez-Mejia, M., Ward, K.M., and Kapp, P., 2016, Magmatic history and crustal genesis of South America: Constraints from U-Pb ages and Hf isotopes of detrital zircons in modern rivers: Geosphere, v. 12, p. 1532–1555, https://doi.org/10.1130/GES01315.1.

Pilger, R.H., 1981, Plate reconstructions, aseismic ridges, and low angle subduction beneath the Andes: Geological Society of America Bulletin, v. 92, p. 448–456, https://doi.org/10.1130/0016-7606(1981)92<448:PRARAL>2.0.CO;2.

Pilger, R.H., 1984, Cenozoic plate kinematics, subduction and magmatism: South American Andes: Journal of the Geological Society [London], v. 141, p. 793–802, https://doi.org/10.1144/gsjgs.141.5.0793.

Pilger, R.H., 2018, Andean Radiometric Database: https://www.researchgate.net/profile/Rex_Pilger2 (accessed February 2019).

Pinto, L., Alarcón, P., Morton, A., and Naipauer, M., 2018, Geochemistry of heavy minerals and U-Pb detrital zircon geochronology in the Manantiales Basin: Implications for Frontal Cordillera uplift and foreland basin connectivity in the Andes of central Argentina: Palaeogeography, Palaeoclimatology, Palaeoecology, v. 492, p. 104–125, https://doi.org/10.1016/j.palaeo.2017.12.017.

Piquer, J., Hollings, P., Rivera, O., Cooke, D.R., Baker, M., and Testa, F., 2017, Along-strike segmentation of the Abanico Basin, central Chile: New chronological, geochemical and structural constraints: Lithos, v. 268–271, p. 174–197, https://doi.org/10.1016/j.lithos.2016.10.025.

Poma, S., Zappettini, E.O., Quenardelle, S., Santos, J.O., Koukharsky, M., Belousova, E., and McNaughton, N., 2014, Geoquímica, dataciones U-Pb SHRIMP sobre circón e isótopos de Hf del magmatismo gondwánico en el NW de Argentina: Petrogénesis e implicancias geodinámicas: Andean Geology, v. 41, p. 267–292, https://doi.org/10.5027/andgeoV41n2-a01.

Porter, R., Gilbert, H., Zandt, G., Beck, S., Warren, L., Calkins, J., Alvarado, P., and Anderson, M., 2012, Shear wave velocities in the Pampean flat-slab region from Rayleigh wave tomography: Implications for slab and upper mantle hydration: Journal of Geophysical Research–Solid Earth, v. 117, B11301, https://doi.org/10.1029/2012JB009350.

Ramos, V.A., 2004, Cuyania, an exotic block to Gondwana: Review of a historical success and the present problems: Gondwana Research, v. 7, p. 1009–1026, https://doi.org/10.1016/S1342-937X(05)71081-9.

Ramos, V.A., 2009, Anatomy and global context of the Andes: Main geologic features and the Andean orogenic cycle, *in* Kay, S.M., Ramos, V.A., and Dickinson, W.R., eds., Backbone of the Americas: Shallow Subduction, Plateau Uplift, and Ridge and Terrane Collision: Geological Society of America Memoir 204, p. 31–65, https://doi.org/10.1130/2009.1204(02).

Ramos, V.A., 2010, The Grenville-age basement of the Andes: Journal of South American Earth Sciences, v. 29, p. 77–91, https://doi.org/10.1016/j.jsames.2009.09.004.

Ramos, V.A., and Folguera, A., 2009, Andean flat-slab subduction through time, *in* Murphy, J.B., et al., eds., Ancient Orogens and Modern Analogues: Geological Society [London] Special Publication 327, p. 31–54, https://doi.org/10.1144/SP327.3.

Ramos, V.A., and Kay, S.M., 1991, Triassic rifting and associated basalts in the Cuyo basin, central Argentina, *in* Harmon, R.S., and Rapela, C.W., eds., Andean Magmatism and its Tectonic Setting: Geological Society of America Special Paper 265, p. 79–92, https://doi.org/10.1130/SPE265-p79.

Ramos, V.A., Jordan, T.E., Allmendinger, R.W., Kay, S.M., Cortés, J.M., and Palma, M., 1984, Chilenia: Un terreno alóctono en la evolución paleozoica de los Andes centrales: Congreso Geológico Argentino, 9th, Bariloche, Argentina, Abstracts, v.2, p. 84–106.

Ramos, V.A., Jordan, T.E., Allmendinger, R.W., Kay, S.M., Cortes, J.M., and Palma, M., 1986, Paleozoic terranes of the central Argentine-Chilean Andes: Tectonics, v. 5, p. 855–880, https://doi.org/10.1029/TC005i006p00855.

Ramos, V.A., Cristallini, E.O., and Perez, D.J., 2002, The Pampean flat-slab of the Central Andes: Journal of South American Earth Sciences, v. 15, p. 59–78, https://doi.org/10.1016/S0895-9811(02)00006-8.

Ramos, V.A., Litvak, V.D., Folguera, A., and Spagnuolo, M., 2014, An Andean tectonic cycle: From crustal thickening to extension in a thin crust (34°–37°SL): Geoscience Frontiers, v. 5, p. 351–367, https://doi.org/10.1016/j.gsf.2013.12.009.

Ranero, C.R., von Huene, R., Weinrebe, W., and Reichert, C., 2006, Tectonic processes along the Chile convergent margin, *in* Oncken, O., Chong, G., Franz, G., Giese, P., Götze, H., Ramos, V.A., Strecker, M.R., and Wigger, P., eds., The Andes: Berlin, Springer, p. 91–121, https://doi.org/10.1007/978-3-540-48684-8_5.

Rapalini, A.E., 2018, The assembly of western Gondwana: Reconstruction based on paleomagnetic data, *in* Siegesmund, S., ed., Geology of Southwest Gondwana: Cham, Switzerland, Springer, p. 3–18, https://doi.org/10.1007/978-3-319-68920-3_1.

Rapela, C.W., Verdecchia, S.O., Casquet, C., Pankhurst, R.J., Baldo, E.G., Galindo, C., Murra, J.A., Dahlquist, J.A., and Fanning, C.M., 2016, Identifying Laurentian and SW Gondwana sources in the Neoproterozoic to early Paleozoic metasedimentary rocks of the Sierras Pampeanas: Paleogeographic and tectonic implications: Gondwana Research, v. 32, p. 193–212, https://doi.org/10.1016/j.gr.2015.02.010.

Rapela, C.W., Pankhurst, R.J., Casquet, C., Dahlquist, J.A., Fanning, C.M., Baldo, E.G., Galindo, C., Alasino, P.H., Ramacciotti, C.D., Verdecchia, S.O., and Murra, J.A., 2018, A review of the Famatinian Ordovician magmatism in southern South America: Evidence of lithosphere reworking and continental subduction in the early proto-Andean margin of Gondwana: Earth-Science Reviews, v. 187, p. 259–285, https://doi.org/10.1016/j.earscirev.2018.10.006.

Rossel, P., Oliveros, V., Ducea, M.N., Charrier, R., Scaillet, S., Retamal, L., and Figueroa, O., 2013, The early Andean subduction system as an analog to island arcs: Evidence from across-arc geochemical variations in northern Chile: Lithos, v. 179, p. 211–230, https://doi.org/10.1016/j.lithos.2013.08.014.

Royden, L.H., 1993, The tectonic expression of slab pull at continental convergent boundaries: Tectonics, v. 12, p. 303–325, https://doi.org/10.1029/92TC02248.

Rubatto, D., 2017, Zircon: The metamorphic mineral: Reviews in Mineralogy and Geochemistry, v. 83, p. 261–295, https://doi.org/10.2138/rmg.2017.83.9.

Rutland, R.W.R., 1971, Andean orogeny and ocean floor spreading: Nature, v. 233, p. 252–255, https://doi.org/10.1038/233252a0.

Sato, A.M., Llambías, E.J., Basei, M.A., and Castro, C.E., 2015, Three stages in the late Paleozoic to Triassic magmatism of southwestern Gondwana, and the relationships with the volcanogenic events in coeval basins: Journal of South American Earth Sciences, v. 63, p. 48–69, https://doi.org/10.1016/j.jsames.2015.07.005.

Schellart, W.P., 2017, Andean mountain building and magmatic arc migration driven by subduction-induced whole mantle flow: Nature Communications, v. 8, p. 2010, https://doi.org/10.1038/s41467-017-01847-z.

Schellart, W.P., 2020, Control of subduction zone age and size on flat slab subduction: Frontiers in Earth Science, v. 8, p. 1–18, https://doi.org/10.3389/feart.2020.00026.

Schellart, W.P., Freeman, J., Stegman, D.R., Moresi, L., and May, D., 2007, Evolution and diversity of subduction zones controlled by slab width: Nature, v. 446, p. 308–311, https://doi.org/10.1038/nature05615.

Schoene, B., 2014, U-Th-Pb geochronology, *in* Holland, H.D., and Turekian, K.K., eds., Treatise on Geochemistry: Volume 4: The Crust (2nd ed.): Amsterdam, Netherlands, Elsevier, Reference Module in Earth Systems and Environmental Sciences, p. 341–378.

Schurr, B., Asch, G., Rietbrock, A., Trumbull, R., and Haberland, C., 2003, Complex patterns of fluid and melt transport in the central Andean subduction zone revealed by attenuation tomography: Earth and Planetary Science Letters, v. 215, p. 105–119, https://doi.org/10.1016/S0012-821X(03)00441-2.

Schwartz, J.J., Gromet, L.P., and Miro, R., 2008, Timing and duration of the calc-alkaline arc of the Pampean orogeny: Implications for the late Neoproterozoic to Cambrian evolution of western Gondwana: The Journal of Geology, v. 116, p. 39–61, https://doi.org/10.1086/524122.

Servicio Geológico Minero (SEGEMAR), 1999, Geologia Argentina: Buenos Aires, Argentina, SEGEMAR, scale 1:3,000,000, digital version, CD-ROM.

Servicio Geológico Minero (SEGEMAR), 2012, Sistema de Información Geográfica del Servicio Geológico Minero Argentino: Buenos Aires, Argentina, SEGEMAR, sig.segemar.gov.ar (accessed June 2018).

Servicio Nacional de Geología y Minería (Sernageomin), 2003, Mapa Geologico de Chile: Version Digital: Sernageomin Publicación Geológica Digital 4, scale 1:1,000,000.

Seton, M., Müller, R.D., Zahirovic, S., Gaina, C., Torsvik, T., Shepard, G., Talsma, A., Gurnis, M., Turner, M., Maus, S., and Chandler, M., 2012, Global continental and ocean basin reconstructions since 200 Ma: Earth-Science Reviews, v. 113, p. 212–270, https://doi.org/10.1016/j.earscirev.2012.03.002.

Seymour, N.M., Singleton, J.S., Mavor, S.P., Gomila, R., Stockli, D.F., Heuser, G., and Arancibia, G., 2020, The relationship between magmatism and deformation along the intra-arc strike-slip Atacama fault system, northern Chile: Tectonics, v. 39, no. 3, https://doi.org/10.1029/2019TC005702.

Sims, J.P., Ireland, T.R., Camacho, A., Lyons, P., Pieters, P.E., Skirrow, R.G., Stuart-Smith, P.G., and Miró, R., 1998, U-Pb, Th-Pb and Ar-Ar geochronology from the southern Sierras Pampeanas, Argentina: Implications for the Palaeozoic tectonic evolution of the western Gondwana margin: Geological Society [London] Special Publication 142, p. 259–281, https://doi.org/10.1144/GSL.SP.1998.142.01.13.

Sláma, J., Košler, J., Condon, D.J., Crowley, J.L., Gerdes, A., Hanchar, J.M., Horstwood, M.S.A, Morris, G., Nasdala, L., Norberg, N., Schaltegger, U., Schoene, B., Tubrett, M., and Whitehouse, M.J., 2008, Plešovice zircon—A new natural reference material for U-Pb and Hf isotopic microanalysis: Chemical Geology, v. 249, p. 1–35, https://doi.org/10.1016/j.chemgeo.2007.11.005.

Spencer, C.J., Murphy, J.B., Hoiland, C.W., Johnston, S.T., Mitchell, R.N., and Collins, W.J., 2019, Evidence for whole mantle convection driving Cordilleran tectonics: Geophysical Research Letters, v. 46, p. 4239–4248, https://doi.org/10.1029/2019GL082313.

Stern, C.R., 2011, Subduction erosion: Rates, mechanisms, and its role in arc magmatism and the evolution of the continental crust and mantle: Gondwana Research, v. 20, p. 284–308, https://doi.org/10.1016/j.gr.2011.03.006.

Storey, B.C., 1995, The role of mantle plumes in continental breakup: Case histories from Gondwanaland: Nature, v. 377, p. 301–308, https://doi.org/10.1038/377301a0.

Sundell, K., Saylor, J.E., and Pecha, M., 2019, Provenance and recycling of detrital zircons from Cenozoic Altiplano strata and the crustal evolution of western South America from combined U-Pb and Lu-Hf isotopic analysis, *in* Horton, B.K., and Folguera, A., eds., Andean Tectonics: Amsterdam, Netherlands, Elsevier, p. 363–397, https://doi.org/10.1016/B978-0-12-816009-1.00014-9.

Taylor, G.K., Grocott, J., Pope, A., and Randall, D.E., 1998, Mesozoic fault systems, deformation and fault block rotation in the Andean forearc: A crustal scale strike-slip duplex in the Coastal Cordillera of northern Chile: Tectonophysics, v. 299, p. 93–109, https://doi.org/10.1016/S0040-1951(98)00200-5.

Thomas, W.A., Astini, R.A., Mueller, P.A., and McClelland, W., 2015, Detrital-zircon geochronology and provenance of the Ocloyic synorogenic clastic wedge, and Ordovician accretion of the Argentine Precordillera terrane: Geosphere, v. 11, p. 1749–1769, https://doi.org/10.1130/GES01212.1.

Torsvik, T.H., Rousse, S., Labails, C., and Smethurst, M.A., 2009, A new scheme for the opening of the South Atlantic Ocean and the dissection of an Aptian salt basin: Geophysical Journal International, v. 177, p. 1315–1333, https://doi.org/10.1111/j.1365-246X.2009.04137.x.

Trumbull, R.B., Riller, U., Oncken, O., Scheuber, E., Munier, K., and Hongn, F., 2006, The time-space distribution of Cenozoic volcanism in the south-central Andes: A new data compilation and some tectonic implications, *in* Oncken, O., et al., eds., The Andes: Active Subduction Orogeny: Berlin, Springer, p. 29–43, https://doi.org/10.1007/978-3-540-48684-8_2.

Vásquez, P., Glodny, J., Franz, G., Frei, D., and Romer, R.L., 2011, Early Mesozoic plutonism of the Cordillera de la Costa (34°–37°S), Chile: Constraints on the onset of the Andean orogeny: The Journal of Geology, v. 119, p. 159–184, https://doi.org/10.1086/658296.

Vergara, M., Levi, B., Nystrom, J.O., and Cancino, A., 1995, Jurassic and Early Cretaceous island arc volcanism, extension, and subsidence in the Coast Range of central Chile: Geological Society of America Bulletin, v. 107, p. 1427–1440, https://doi.org/10.1130/0016-7606(1995)107<1427:JAECIA>2.3.CO;2.

Vermeesch, P., 2018, IsoplotR: A free and open toolbox for geochronology: Geoscience Frontiers, v. 9, p. 1479–1493, https://doi.org/10.1016/j.gsf.2018.04.001.

Vervoort, J.D., and Blichert-Toft, J., 1999, Evolution of the depleted mantle: Hf isotope evidence from juvenile rocks through time: Geochimica et Cosmochimica Acta, v. 63, no. 3–4, p. 533–556, https://doi.org/10.1016/S0016-7037(98)00274-9.

Wells, M.L., Hoisch, T.D., Cruz-Uribe, A.M., and Vervoort, J.D., 2012, Geodynamics of synconvergent extension and tectonic mode switching: Constraints from the Sevier-Laramide orogen: Tectonics, v. 31, TC1002, https://doi.org/10.1029/2011TC002913.

Willner, A.P., Gerdes, A., and Massonne, H.J., 2008, History of crustal growth and recycling at the Pacific convergent margin of South America at latitudes 29°–36°S revealed by a U-Pb and Lu-Hf isotope study of detrital zircon from late Paleozoic accretionary systems: Chemical Geology, v. 253, p. 114–129, https://doi.org/10.1016/j.chemgeo.2008.04.016.

Willner, A.P., Massonne, H.J., Ring, U., Sudo, M., and Thomson, S.N., 2012, *P-T* evolution and timing of a late Palaeozoic fore-arc system and its heterogeneous Mesozoic overprint in north-central Chile (latitudes 31–32°S): Geological Magazine, v. 149, p. 177–207, https://doi.org/10.1017/S0016756811000641.

Wu, F.Y., Yang, Y.H., Xie, L.W., Yang, J.H., and Xu, P., 2006, Hf isotopic compositions of the standard zircons and baddeleyites used in U-Pb geochronology: Chemical Geology, v. 234, p. 105–126, https://doi.org/10.1016/j.chemgeo.2006.05.003.

Xia, X., Sun, M., Geng, H., Sun, Y., Wang, Y., and Zhao, G., 2011, Quasi-simultaneous determination of U-Pb and Hf isotope compositions of zircon by excimer laser-ablation multiple-collector ICPMS: Journal of Analytical Atomic Spectrometry, v. 26, p. 1868–1871, https://doi.org/10.1039/c1ja10116a.

Yakymchuk, C., Kirkland, C.L., and Clark, C., 2018, Th/U ratios in metamorphic zircon: Journal of Metamorphic Geology, v. 36, no. 6, p. 715–737, https://doi.org/10.1111/jmg.12307.

Yáñez, G.A., Ranero, C.R., Huene, R., and Díaz, J., 2001, Magnetic anomaly interpretation across the southern Central Andes (32–34°S): The role of the Juan Fernández Ridge in the late Tertiary evolution of the margin: Journal of Geophysical Research–Solid Earth, v. 106, p. 6325–6345, https://doi.org/10.1029/2000JB900337.